BOLT BERANEK AND NEWMAN INC

CONSULTING • DEVELOPMENT • RESEARCH

Report No. 1769

WAVENUMBER-FREQUENCY SPECTRA OF TURBULENT-BOUNDARY-LAYER PRESSURE MEASURED BY MICROPHONE ARRAYS

By
William K. Blake and David M. Chase

Contract No. Nonr 3468(00)
Task 2.3
BBN Job No. 11295

25 April 1969

Submitted to:

Acoustics Branch, Code 468
Office of Naval Research
Washington, D.C. 20360

Attention: Mr. Marvin Lasky

WAVENUMBER-FREQUENCY SPECTRA OF TURBULENT-BOUNDARY-LAYER PRESSURE MEASURED BY MICROPHONE ARRAYS

By
William K. Blake and David M. Chase

Contract No. Nonr 3468(00)

Task 2.3
Flow Noise Evaluation

Report No. 1769

Job No. 11295

25 April 1969

Submitted to:

Acoustics Branch, Code 468
Office of Naval Research
Washington, D.C. 20360
Attention: Mr. Marvin Lasky

Submitted by:

Bolt Beranek and Newman Inc.
50 Moulton Street
Cambridge, Massachusetts 02138

ABSTRACT

Measurements of frequency spectra of pressure along a wind-tunnel wall have been made by single microphones and by a longitudinal array of four flush 0.8-inch circular microphones connected with alternating and with common phase. The alternating-phase array was designed to suppress by its wavenumber filtering the background acoustic duct noise at frequencies near 3 kHz. The measured levels set upper limits on low-wavenumber boundary-layer pressure. Analysis indicates that the high-wavenumber (convective) contribution in this frequency range was probably negligible, but it could not be definitely established whether background noise dominated the spectra or whether the upper bound set on low-wavenumber boundary-layer noise is a close one. On assumption of wavenumber independence in most of the pertinent low-wavenumber domain, an upper bound is given for the wavenumber spectral density of boundary-layer pressure, and its generalization by assumption of δ_*-independence is discussed. At lower frequencies, in identifiable domains where single-microphone and array spectra are dominated by the convective wavenumber component of boundary-layer pressure, satisfactory agreement is found with theoretical predictions based on current knowledge of the spectral density in the convective-wavenumber domain and on a measured facial sensitivity distribution for the microphone. In general, salient features of the array spectra correlate well with expectation, and the array technique is demonstrated to be a useful one for the subject purposes.

FOREWORD

Participation by Dr. Robert D. Collier in planning the experimental work reported here is gratefully acknowledged. The experiment was conducted by the first coauthor of this report (WKB).

TABLE OF CONTENTS

LIST OF SYMBOLS

ρ	fluid mass density (air in wind tunnel)
ν	kinematic viscosity
c	sound velocity
$\bar{x}=(x_1,x_3)$	position vector in plane of wall (x_1 streamwise)
$\bar{k}=(k_1,k_3)$	wavenumber vector
y	normal distance from wall
ω	radian frequency
U_∞	free-stream flow velocity
q	dynamic pressure ($=\rho U_\infty^2/2$)
$U(y)$	mean flow velocity
U_c	effective boundary-layer convection velocity
v_*	boundary-layer friction velocity
δ^*	displacement thickness
$\Phi(\bar{k},\omega)$	wavenumber-frequency spectral density of pressure on wall
$\Phi(\omega)$	frequency spectrum of pressure at point on wall
$\lvert F(\omega)\rvert^2$	normalized microphone frequency response
$\Phi_M(\omega)$	frequency spectrum of area-averaged pressure measured by single microphone
$\Phi_A(\omega)$	frequency spectrum of wavenumber-filtered pressure measured by array of microphones
$\Delta\omega/\omega$	relative bandwidth of fractional-octave filter
$\psi_M(\omega)$	$[=(\Delta\omega/2\pi)\Phi_M(\omega)]$ single-microphone spectrum measured in relative bandwidth $\Delta\omega/\omega$.
$\hat{\Phi}(k,\omega)$	average over angle of $\bar{k}$ of boundary-layer contribution to $\Phi(\bar{k},\omega)$

LIST OF SYMBOLS (Continued)

$\Phi_{M_-}(\omega), \Phi_{A_-}(\omega)$	low-wavenumber boundary-layer pressure contribution to $\Phi_M(\omega), \Phi_A(\omega)$, respectively
$\hat{\Phi}_-(\omega)$	weighted average of $\hat{\Phi}(k,\omega)$ over low-wavenumber range pertinent to single microphone
$\Phi_{m_-}(\omega)$	boundary-layer contribution to $\Phi_{A_-}(\omega)$ from vicinity of major wavenumber lobe m of array response
$\tilde{\Phi}_m(\omega)$	weighted average over k_3 [pertinent to $\Phi_{m_-}(\omega)$] of boundary-layer part of $\Phi(k_m,k_3,\omega)$, where k_m is wavenumber of m^{th} major-lobe peak in array response
R	radius of sensitive area of circular microphones
$S(\bar{x})$	normalized facial sensitivity distribution of microphone
$\lvert H(\bar{k})\rvert^2$	wavenumber filter expressing area averaging by single microphone characterized by $S(\bar{x})$
B,α,β	constants in approximate function fitted to measured $S(\bar{x})$ for microphones used in present array measurements
c_o	(=5.93) coefficient related to function approximating microphone facial response
R_e	effective radius of array microphones with reference to low-wavenumber pressure components
R_o	radius of arbitrary pressure sensor with uniform facial response
N	number of elements in linear array
d	center spacing of elements in array
$\lvert A(\bar{k})\rvert^2$	array wavenumber filter (assuming arbitrary identical elements)

Ω	$(=\omega R/U_\infty)$ dimensionless frequency based on element radius
Δ_M	$[= 2\pi(\omega/\Delta\omega)\psi_M(\omega)/\rho^2 U_\infty^4]$ dimensionless pressure spectrum measured by single microphone in relative bandwidth $\Delta\omega/\omega$.
Δ_A	same as Δ_M for measurement by array of microphones
A_o	coefficient in conjectured δ^*-independent, wavenumber-independent spectral density of boundary-layer pressure at low wavenumbers (Eq. 22)
a_o	same as A_o with v_* instead of U_∞ as velocity scale
C, G_o, A	numerical constants measuring wavenumber-frequency spectral density of boundary-layer pressure in the convective ridge, as given by space-time isotropic, scale-independent form Eq. 34 $[G_o=2\pi C^2\gamma^{-1}s,\ A=G_o(v_*/U_\infty)^4]$
v	$(=sv_*)$ parameter in Eq. 34 expressing velocity dispersion relative to mean convection velocity
a^{-1}	$(=b\delta^*)$ parameter in Eq. 34 measuring largest scale of correlation in streamwise (x_1) direction
γ	ratio of largest scale of transverse to streamwise correlation at fixed time
α_o	$=[1+(\omega/aU_c)^{-2}]^{1/2}$

1. INTRODUCTION

Past investigations of turbulent-boundary-layer wall-pressure fluctuations have proceeded mainly by measurements of frequency spectra of average pressure on single elements of various sizes and by measurements of narrow- or broad-band correlations. In the present work in the BBN wind tunnel, the technique of using instead a coherent array of (four) elements was implemented for measurements of frequency spectra directed mainly toward establishing the wavenumber-frequency spectrum of boundary-layer pressure in the low-wavenumber domain.

In brief preliminary summary, the technique has been successfully demonstrated and an upper limit placed on the low-wavenumber contribution to boundary-layer noise. In a certain frequency range the alternating-phase array discriminated effectively against background duct noise; nevertheless, it has not been excluded that this spurious source was still dominant. A contribution from high-wavenumber (convective) boundary-layer pressure was also present, but analysis suggests that this was relatively small.

On the basis of previous measurements of turbulent boundary-layer pressure, as well as the rudimentary kinematics of convection of pressure-generating eddies, it is recognized that the joint wavenumber-frequency spectrum of wall pressure, say, $\Phi(\bar{k},\omega)$ [where $\bar{k}=(k_1,k_3)$], is sharply peaked with regard to streamwise wavenumbers (k_1) at a value $k_1=\omega/U_c$, where U_c is a convection velocity weakly dependent on frequency and equal to some major fraction of the free-stream velocity U_∞. The decrease with spanwise wavenumber ($|k_3|$) is much slower, so that $\Phi(\bar{k},\omega)$

possesses a "convective ridge" centered at $(k_1,k_3)\approx(\omega/U_c,0)$ and oriented normal to the flow. Well removed from this convective domain, in a low-wavenumber domain defined by $k<<\omega/U_\infty$, $\Phi(\bar{k},\omega)$ fails to vanish only on account of improbably high fluctuating convection velocities and distortion and decay of eddies. This latter domain, though hitherto subjected to little conclusive investigation, has great importance in various instances where the system response heavily weights the low wavenumbers.

Correlations and frequency spectra of pressure on individual elements have been measured by various investigators, including Bull (1967), Willmarth and Wooldridge (1962), and Blake (1969). The cross-spectral density of pressure on pairs of elements have also been measured in considerable detail, for example by Bull (1967), Blake (1969), and Wills (1967). These latter measurements may be used to compute approximately, by Fourier inversion, the wavenumber-frequency spectrum of pressure; the measured cross-spectra, however, are dominated by the contribution from the convective domain, so that no reliable inference is possible concerning the spectral density at low wavenumbers. Boundary-layer pressure spectra on single large elements, on the other hand, because of the weighting represented by area-averaging, may be dominated by the low-wavenumber contributions, but inference of the low-wavenumber level from such measurements is ordinarily questionable on account of the relatively low values of $\Phi(\bar{k},\omega)$ and the possible contamination by spurious background acoustic noise or noise associated with vibration of the flow-bounding walls.

What is needed is a more discriminating wavenumber filter that largely rejects a spurious acoustic field. The use of alternating-phased, or more generally of phase-differenced (steered), arrays of elements with outputs added coherently constitutes a powerful tool for this purpose. This technique was originally proposed at BBN by Dr. James E. Barger and pursued in the present work. A description of the use of such an array system has been given by Maidanik and Jorgensen (1967).

2. PRESSURE SPECTRA WAVENUMBER-FILTERED BY A MICROPHONE ARRAY

In this section the method of wavenumber-frequency filtering is supported mathematically. General relations and definitions are presented with minimal derivations in view of their availability in cited references.

The space-time correlation of the wall pressures at point $\bar{x}$, time t and point $\bar{x}+\bar{r}$, time $t+\tau$ can be written as

$$R(\bar{r},\tau) = \langle p(\bar{x},t)p(\bar{x}+\bar{r},t+\tau)\rangle \ , \qquad (1)$$

where the brackets denote time averages for this (assumed) spatially homogeneous and temporally stationary field. The wavenumber-frequency spectral density is the Fourier transform of the space-time correlation, expressed as

$$\Phi(\bar{k},\omega) = (2\pi)^{-3} \iiint R(\bar{r},\tau)e^{-i[\bar{k}\cdot\bar{r}-\omega\tau]}d^2\bar{r}d\tau \ , \qquad (2)$$

where integrals run over the infinite domain unless otherwise indicated. The frequency spectral density of wall-pressure fluctuations is

$$\Phi(\omega) = \frac{1}{2\pi}\int R(0,\tau)e^{i\omega\tau}d\tau = \iint \Phi(\bar{k},\omega)d^2\bar{k} \ . \qquad (3)$$

The measurement of the frequency spectral density of wall pressure fluctuations involves the influence of the microphone facial sensitivity distribution $S(\bar{x})$ in averaging small wavelength wall-pressure components. Thus, assuming instantaneous response, when subject to a pressure field $p(\bar{x},t)$, the microphone measures an area-averaged pressure

$$q(t) = \iint S(\bar{x})p(\bar{x},t)d^2\bar{x}, \quad \text{where } \iint S(\bar{x})d^2\bar{x}=1 .$$

The response function, $|H(\bar{k})|^2$, expresses the facial distribution as a wavenumber filter and is defined by

$$H(\bar{k}) = \iint S(\bar{x})e^{-i\bar{k}\cdot\bar{x}}d^2\bar{x} , \tag{4}$$

where $\bar{x}$ may be measured from the center of the face and $S(\bar{x})$ vanishes for $\bar{x}$ outside the sensitive area. The frequency spectrum of area-averaged pressure measured by a single hydrophone is then given by

$$\Phi_M(\omega) = \iint\Phi(\bar{k},\omega)|H(\bar{k})|^2d^2\bar{k} \tag{5}$$

(e.g., see Uberoi and Kovasznay 1953, Chandiramani 1968). If the condition of instantaneous response is relaxed but the time response is separable from the facial response and characterized by a frequency filter $|F(\omega)|^2$, Eq. 5 remains applicable provided $\Phi_M(\omega)$ is understood to refer to the spectrum properly calibrated by division of the actual output spectrum by $s_o^2|F(\omega)|^2$, where s_o is a sensitivity constant.

With a calibrated array of identical microphones, the measured spectrum analogous to Eq. 5 is given by

$$\Phi_A(\omega) = \iint\Phi(\bar{k},\omega)|H(\bar{k})|^2|A(\bar{k})|^2d^2\bar{k} , \tag{6}$$

where $|A(\bar{k})|^2$ is the array wavenumber response function (e.g., see Maidanik and Jorgensen 1967). In the special case of interest, an N-element line array with equal spacing-vector $\bar{d}$ between adjacent element centers and no time delay between elements, this function may be written

$$|A(\bar{k})|^2 = N^{-2} \left| \sum_{n=0}^{N-1} a_n \exp(-in\bar{k}\cdot\bar{d}) \right|^2 \qquad (7)$$

in which the coefficients a_n, in the instance of no shading of element weights, are given by

$$a_n = \begin{cases} 1, & \text{common-phase array} \\ (-)^n, & \text{alternating-phase array.} \end{cases}$$

For an array aligned with the x_1 direction, Eq. (7) then becomes

$$|A(\bar{k})|^2 = \begin{cases} \dfrac{\sin^2(\frac{1}{2}Nk_1d)}{N^2\sin^2(\frac{1}{2}k_1d)}, & \text{common phase} \\ \dfrac{\sin^2[\frac{1}{2}N(k_1d-\pi)]}{N^2\cos^2(\frac{1}{2}k_1d)}, & \text{alternating phase} \end{cases} . \qquad (8)$$

The response patterns for the two phase conditions are identical but shifted relative to one another by π/d in k_1. The number of minor lobes between adjacent major lobes is N-2. Fig. 1 shows the array responses for the case N=4 of the present measurements. It is to be emphasized that $|A(\bar{k})|^2$ is not influenced by the response of the individual microphones (assumed identical); the latter response is embodied solely in $|H(\bar{k})|^2$.

The alternating-phase array with N=4 has a null in its response at $k_1=\pm\pi/2d$ and, furthermore, has no major lobe in the interval $-\pi/2d<k_1<\pi/2d$ but rather only minor lobes with peaks at $k_1=\pm\pi/4d$ that are lower by 11 dB. Therefore, at frequencies such that $\omega/c\lesssim\pi/2d$, where c is the sound velocity in the flowing medium,

acoustic fields (for which $k \leq \omega/c$) are substantially attenuated by the array. More important, to the extent that spurious acoustic noise originates in the wind-tunnel blower and propagates up the tunnel purely via a longitudinal wave with $k_1 = -\omega/c$, at that particular frequency given by $\omega/c = \pi/2d$ the array response to such noise is nil. This same null occurs in the case of the common-phase array, but the latter array presents a major-lobe rather than only a minor-lobe response to non-longitudinal sound waves having $|k_1| < \omega/c$.

The response $|H(\bar{k})|^2$ has an upper bound that decreases with kR for $kR \gtrsim \pi$ and thus attenuates the high-wavenumber components of the pressure field; in particular, when $\omega R/U_\infty \geq \pi$, it attenuates the convective component ($k_1 \approx \omega/U_c$) of the boundary-layer pressure. Hence the array is most sensitive at the lowest-k major lobes of the comb filters (8), i.e., at $k_1 \approx \pm\omega\pi/d$ for alternating phase and at $k_1 = 0$ and $k_1 \approx \pm 2\pi/d$ for common phase. The contribution from the next higher major lobes for the alternating-phase array, $k_1 = \pm 3\pi/d$, can be nearly eliminated by choice of transducer radius (and facial response) such that $H(\bar{k}) = 0$ at $k = 3\pi/d$. In such case, assuming that the attenuation of the background acoustic field and the high-wavenumber boundary-layer pressure field suffices, the alternating-phase array measurement yields a weighted integral over k_3 of the boundary-layer pressure spectrum $\Phi(\bar{k},\omega)$ at a relatively well defined, low (nonconvective) streamwise wavenumber such that $|k_1| \approx \pi/d$.

For a circular element of radius R and uniform facial sensitivity, we have

$$|H(\bar{k})|^2 = [2J_1(kR)/kR]^2 \qquad (k^2 \equiv k_1^2 + k_3^2) \quad , \tag{9}$$

whose upper bound decreases for $kR \geq \pi$ as $(kR)^{-3}$. In this instance the condition $H(\bar{k})=0$ at $k=3\pi/d$ yields $(3\pi/d)R=3.8$ or $d/R=2.5$. Figs. 2a and 2b show the corresponding computed function $|A(k_1)|^2|H(k_1)|^2$ at $k_3=0$ for both phase relations. The microphones actually used had a facial sensitivity significantly nonuniform, as discussed in Section 5.2.

3. DESCRIPTION OF THE MICROPHONE ARRAY

The measurements were made using an array of four Brüel & Kjaer No. 4131 1-in. diameter microphones with 1.06-in. separations. An area of the microphone diaphragm at least 0.8 in. in diameter is sensitive to pressure (Brüel and Rasmussen 1959).

The design of the array system was guided by three factors:

1) Simplicity in construction
2) Cost of instrumentation
3) Desired suppression of high-wavenumber, convective boundary-layer contribution to measured spectra at high frequencies by area averaging by large microphones.

The first two factors were important because the experiments were considered as preliminary studies. Development of an inexpensive array system was considered sufficient to indicate the usefulness of the array approach to the boundary-layer measurements. The third factor reflects the objective of setting a minimum upper limit on the low-wavenumber boundary-layer contribution to array spectra in the frequency range of high discrimination against background acoustic noise.

The four B&K microphones were flush mounted in a plexiglass support, which was mounted in the wind tunnel with the microphones aligned in the streamwise direction. (The description of the tunnel is in Section 3.1.) The microphones were driven by four B&K No. 2801 power supplies, the outputs of which led to a phase control circuit and transformer to provide the common and alternating phase characteristic for the array.

The phase-control circuit put the 200-ohm impedance outputs from the power supply transformers in series. The phase shifting was accomplished by alternating the voltage level (positive or negative) with respect to the common ground. The voltage level was shifted by using three-way toggle switches, and the combined signal from the power-supply outputs was fed to the high-impedance side of a transformer. The summed output was fed to an Ithaco No. 255-A low-noise, high-gain amplifier.

Frequency analysis was performed using filters of 1/10th-octave bandwidth of a General Radio (G.R.) sound and vibration analyzer No. 1564-A and a G.R. graphic level recorder No. 1521-A.

4. RESULTS OF MEASUREMENTS

4.1 Calibration of the Array Response

The microphones in the array were matched to give identical outputs to a 124 dB (re 0.0002μb) acoustic signal generated by a B&K No. 4220 pistonphone. Variable resistors in the phase circuitry permitted attenuation of the signal generated by the most sensitive microphones in the array so that all microphones could be tuned to give identical outputs to the calibration pressure.

The array response, $|A(\bar{k})|^2$, was determined by passing plane-wave sound over the microphone array. The array was mounted in a plywood panel supported from the ceiling of the BBN anechoic chamber. A ten-inch speaker situated 10 feet from the array was used to generate the sound field. The plane of the array and plywood panel was parallel to the axis of the speaker. The wavenumber of the sound field is $2\pi f/c$, where f is the frequency and c is the speed of sound in air. Fig. 3 shows the measured array response as a function of sound-field frequency after correction for the microphone frequency response and area-averaging effects. Points calculated for the total response function, $s_o^2|A(\bar{k})|^2|H(\bar{k})|^2$, are included.* The common-phase array response was not measured; the calculated points of $s_o^2|A|^2|H|^2$ are shown in Fig. 4. The computation of $|A|^2$ is considered reliable in view of the excellent agreement between measurement and computation shown in Fig. 3 for the alternating-phase array. The frequency responses of the microphones and the speaker efficiency decrease rapidly above 10 kHz so that the array calibration was not possible at high frequencies.

*The microphone response factor was computed for uniform facial response rather than the actual one (see Figs. 15, 16); use of the latter would raise the minor-lobe peak at 10.5 kHz by 2.2 dB and have a decreasing effect at lower frequencies.

The sensitivity of each microphone was determined as -63.12 dB re 1V/μb, and the sensitivity of the major lobe of the alternating-phase array was measured as -51.5 dB. This is consistent with the level as calculated from the array response of Fig. 2a within a ± 1 dB uncertainty in the measurement.

There is nearly complete cancellation of the 3 kHz sound field as would be expected by examining Fig. 2a for the computed alternating- and common-phase array responses. The frequency responses of the microphones were identical up to 6 kHz; they remained constant within 1 dB to 2 kHz, decreased to -1.75 dB at 3 kHz, -3 dB at 4 kHz, and -5 dB at 6 kHz. None of the pressure spectra have been corrected for this decrease in response, but the data analysis is largely confined to frequencies below 3 kHz.

4.2 Boundary Layer Description

The turbulent boundary layer measurements were performed in the BBN wind tunnel facility described by Chandiramani and Blake (1968). Three sides of the test-section ducting were lined with 6-inch thick "Ultrafine" acoustic insulation which diminished the reverberant field in the ducting above about 1 kHz. The boundary layer was formed on the formica-coated test-section bottom and was artificially thickened by covering the first 7-1/2 inches of the panel with coarse sandpaper. The mean velocity profile was measured with an 0.040-inch diameter flattened-tip total-head tube. The velocity data were extracted from readings of total less static head obtained on a slanted tube manometer. The readings were recorded to 0.01 inch of water. The static pressure was obtained with a 0.1-inch I.D. copper tube flush-mounted in the floor of the test section. All

measurements were made at 4.5 feet from the test-section inlet which is the assumed boundary-layer origin. The plate Reynolds number for the measurements, $N_{Rex} = xU_\infty/\nu$, ranged from 10^5 to 1.7 (10^5) for U_∞ = 40 ft/sec to 63 ft/sec.

Fig. 5 shows the mean velocity profile (U/U_∞ vs. $y/\delta_{0.99}$) for the three free-stream velocities considered in these measurements. The boundary-layer thickness was determined as the distance from the wall at which $U(y) = 0.99U_\infty$. The displacement thickness was determined by mechanical integration of the mean velocity profile according to the definition

$$\delta^* = \int_0^\infty (1-U/U_\infty)dy \ .$$

The outer mean flows of the boundary layers follow quite closely the velocity-defect law derived from Coles' wake law. This law may be written

$$\frac{U_\infty - U}{v_*} = -5.75 \log(y/\delta_{0.99}) + \frac{\Pi}{\kappa}\left[2-w(y/\delta_{0.99})\right] , \qquad (10)$$

where, from Hinze's (1960) curve fitting to Coles' data

$$w(y/\delta) \simeq 1+\sin\left[(2y/\delta-1)\pi/2\right]$$

and $\Pi = 0.55$ for the zero-pressure-gradient boundary layer. κ is the von Kármán universal constant and is given the value of 0.4 by Coles. The agreement between measurements and Eq. 10 in Fig. 6 is very good.

These velocity measurements are of limited extent, but they give evidence that an experimentally reproducible boundary layer flow has been considered. In addition, the measurements indicate that the boundary-layer outer flow is described by the universally applicable velocity-defect law for zero-pressure-gradient boundary layers.

TABLE OF BOUNDARY LAYER PROPERTIES

U_∞(ft/sec)	$\delta_{0.99}$(in.)	δ^*(in.)	v_*/U_∞	$N_{Re\delta^*}$
39.5	1.2	0.184	0.0405	3.6×10^3
51.5	1.25	0.205	0.0401	4.6×10^3
63	1.15	0.184	0.0395	5.7×10^3

4.3 Pressure Spectra Measured by Single Microphones

The frequency spectral density of wall-pressure fluctuations is shown in Fig. 7 in the non-dimensional form

$$\Phi_M(\omega)U_\infty/q^2\delta^* \text{ vs. } \omega\delta^*/U_\infty \qquad (q=\rho U_\infty^2/2).$$

The single-microphone spectrum measurement is represented by the mathematical equivalent in Eq. 5. The spectrum is two sided, i.e.,

$$\langle p^2\rangle = 2\int_0^\infty \Phi(\omega)d\omega \ . \qquad (11)$$

The effect of nonvanishing microphone size on the measured spectrum is shown by comparing the current measurements with those of Blake (1969) and Willmarth and Wooldridge (1962). The present

measurements were made with microphones approximately 0.8 inch and 0.2 inches in diameter (B&K No. 4131 1-inch and B&K No. 4136 1/4-inch condenser microphones respectively). The spectra were measured over a wide range of nominal microphone diameters (D),

$$0.11 < D/\delta^* < 4 \ , \qquad (12)$$

and may be shown qualitatively consistent by applying Corcos' (1963) correction. The flagged points of the current data and the arrows on the spectra of Willmarth and of Blake denote frequencies for which $\omega R/U_c \approx 1$. A Corcos correction of about +3 dB would be required at this frequency. When the Corcos correction is applied to the data, all corrected spectra are spread about the uncorrected Blake (1969) line within ± 3 dB for frequencies less than $\omega\delta^*/U_\infty = 10$.

4.4 Pressure Spectra Measured by Arrays

The measurements obtained with each of the two array configurations, alternating-phase and common-phase, are reported here in this order, and the salient features identified. Detailed analysis is given in Section 5.

The 1/10th-octave pressure levels as filtered by the alternating-phase array are shown in Figs. 8, 9, and 10 for the three flow speeds considered. The corresponding levels measured by a single one-inch microphone are shown for comparison. The array sensitivity used to convert voltage to SPL per

0.0002 μb is that of the major lobe (at 6 kHz in Fig. 3) which is at a wavenumber of $k_1 \simeq 2.75$ in.$^{-1}$. The fractional-octave level for the single-microphone measurements will be denoted by

$$4\pi\psi_M(\omega) = 2 \int_{-\infty}^{\infty} d\omega' \Phi_M(\omega') |G(\omega'-\omega)|^2 \ . \qquad (12.1)$$

(and similarly for the array measurements, with subscript A replacing M), where $|G(\omega'-\omega)|^2$ is the frequency-filter response at ω' when the filter is centered at ω and $|G(0)|^2 = 1$. A bandwidth, $\Delta\omega$, is defined by

$$\Delta\omega = \int_{-\infty}^{\infty} d\omega' |G(\omega'-\omega)|^2 \ .$$

If $\Phi_M(\omega')$ varies little for $\omega'-\omega$ such that $G(\omega'-\omega)$ is appreciable, Eq. 12.1 is approximated by

$$4\pi\psi_M(\omega) = 2\Delta\omega\Phi_M(\omega) \ . \qquad (13)$$

In the present, tenth-octave case we have $\Delta\omega/\omega = 0.0685$, and approximation (13) is expected to be adequate.* Since Φ_M is normalized as in (11), relation (13) reflects normalization of the plotted $4\pi\psi_M(\omega)$ such that mean squared pressure is represented by $\int_0^{\infty} 4\pi\psi_M(\omega) d\omega/\Delta\omega$.

The striking feature of the array pressure levels is the occurrence of peaks labeled (a),(b),(c), and (d). A comparison of Figs. 8 through 10 and Fig. 3 shows clearly that peak (c) is due to background duct noise admitted by the major array lobe at $-k_1 \simeq \pi/d$. This noise consists primarily of plane waves propagated nearly longitudinally; their wavenumber coincides with

*For example, the frequency half-width of the convective peak in the spectral density of turbulent boundary-layer pressure at fixed wavevector, $\bar{k}$, is ~0.1ω; this exceeds Δω even apart from the relative broadening at low frequencies due to integration over the width of the area-averaging and array wavenumber filters.

the major array lobe at the frequency where $\omega/c=\pi/d$, i.e., f=6 kHz. The array and single-microphone measurements yield equal levels near (c), indicating that the width in k_1 of the duct-noise wavenumber spectrum is less than the width ($\sim\pi/2d$) of the major lobe of the array filter.

Peak (a) is due to the convective peak in the wavenumber spectrum of aerodynamic boundary-layer pressure admitted similarly by the major lobe at $k_1\approx\pi/d$. In terms of an effective convection velocity U_c, this coincidence occurs at the frequency where $\omega/U_c\approx\pi/d$. The data for the three free-stream velocities thus yield $U_c\approx0.75U_\infty$ for $\omega\delta^*/U_\infty\approx0.41$. Again the array and single-microphone levels become almost equal near (a), indicating that the width in k_1 of the convective peak in the wavenumber spectrum $\Phi(\bar{k},\omega)$ of boundary-layer pressure at the subject values of $\omega d/U_\infty$ is less than the width of the array major lobe.

Peaks (b) and (d), like (a) and (c), are attributable respectively to duct noise and convective-wavenumber boundary-layer pressure, but in this case admitted by the second major array lobe at $|k_1|\approx3\pi/d$, which is not entirely suppressed by the microphone response $|H(\bar{k})|^2$.

For frequencies above 1 kHz the acoustic lining in the test-section duct efficiently absorbs the reverberant duct noise, leaving mainly longitudinal plane-wave sound, which can be distinguished from aerodynamic wall-pressure fluctuations. At 3 kHz, where $\omega/c=\pi/2d$, the array discriminates against the duct noise (see Fig. 3). Thus the measured pressure levels of Figs. 8 through 10 are depressed in the neighborhood of 3 kHz. It would be hoped that at 3 kHz the levels are primarily due to wall pressure fluctuations in wavenumber bands passed by the filtering array. This central question will be considered in Section 5.

The hollow at about 50 Hz in Figs. 8 through 10 is probably due to coincidence of the convective peak of the wall-pressure wavenumber spectrum with the array response null at $k_1=\pi/2d$. The corresponding condition, $\omega/U_c=\pi/2d$, yields $U_c=0.35U_\infty$ at $\omega\delta^*/U_\infty=0.1$ and $U_c=0.41U_\infty$ at $\omega\delta^*/U_\infty=0.12$ (from Figs. 9 and 10). These low phase velocities are comparable with those measured from cross-spectral densities by Blake (1969). The values obtained here for phase velocities are approximate because the wavenumber for minimum noise is influenced by the contribution of reverberant duct noise. A tendency of the spectra in Figs. 8 through 10 to form maxima at about half the frequency of the minima just mentioned would also be expected, on account of coincidence of the convective peak and the lowest minor lobe where $\omega/U_c=\pi/4d$.

The 1/10th-octave pressure levels as filtered by the common-phase array are shown in Figs. 11, 12, and 13. Voltage levels were converted to pressure levels using the sensitivity of -50 dB re 1v/μb for the first major (k_1=0) lobe (see Fig. 4).

The peak labeled (a), analogous to peak (a) in the alternating-phase measurements, is due to coincidence of the convective peak in the wavenumber spectrum of boundary-layer pressure with the major array lobe at $k_1=2\pi/d$, occurring where $\omega/U_c \simeq 2\pi/d$. This condition yields $U_c \simeq 0.74U_\infty$ at $\omega\delta^*/U_\infty \simeq 0.87$.

The peak (b) is attributable to coincidence of the duct-noise wavenumber with the first minor array lobe, occurring where $\omega/c = 3\pi/4d$, i.e., at f = 4.5 kHz (see Fig. 4).

The measurements show a depression in the level near 3 kHz, where the array discriminates against duct noise, though the levels there are slightly higher than for the alternating-phase array, as discussed further below.

5. DETAILED ANALYSIS

In this section we consider further the question whether the measured array spectra are actually dominated by low-wavenumber turbulent boundary-layer pressure fluctuations in the range of high discrimination against duct noise and against high-wavenumber (convective) boundary-layer noise, and whether, at any rate, the upper limit placed on the low-wavenumber spectral density is usefully low. We also compare the spectra for the arrays and single microphones with the convective contribution estimated by a suitable model of boundary-layer pressure; we thereby attempt to demonstrate consistency, if not improve the determination of the model parameters, in the domain where the convective contribution dominates the spectra, and to estimate this contribution to array spectra in the domain where it may be hoped to be smaller than the low-wavenumber contribution. Due consideration is given to the wavenumber filter corresponding to the actual facial response of the microphones.

5.1 Spurious Acoustic Noise

We consider the possible level of spurious noise in the vicinity of 3 kHz where the arrays most discriminate against it. One indication is provided by the difference in levels at 3 kHz measured by the array and by a single microphone; this difference may be compared with the difference in levels at this frequency in calibration, as implied by the array calibration in Fig. 3. The former difference (10.5 to 12 dB at the three speeds) is much less than the difference in the instance of the calibration signal, so that it is at least not excluded that the array noise level at 3 kHz is much higher than the extant acoustic background on account of the boundary-layer noise contribution, as desired.

On the other hand, the decreased level difference for noise measured during flow relative to that in calibration could be due instead to an angular distribution of the spurious acoustic noise that is less sharply peaked in the longitudinal direction ($-k_1=\omega/c, k_3=0$), and hence less discriminated against at 3 kHz by the array, than is true of the highly longitudinal acoustic field produced by the calibration source in the absence of flow-excited modes in the tunnel. Hence, the smaller difference between the subject levels and the shift of the noise minimum for the alternating-phase array from 3 kHz to a somewhat higher frequency, though encouraging, do not necessarily imply that dominance by spurious acoustic noise is excluded even near 3 kHz.

A possible further indication is provided by comparison of the levels measured by the alternating-phase and common-phase arrays. The difference in measured levels at the three speeds is shown in Fig. 14 for the entire frequency range above 1 kHz. Also shown is the difference predicted for a purely longitudinal accustic field using the theoretical array responses (for the alternating-phase array this closely approximates that measured in calibration, Fig. 3). In this way we use the common-phase measurements to estimate the background noise spectrum for the alternating-phase measurements.*

*An estimated single-microphone background-noise spectrum is shown in Figs. 11-13.

Since the excess of the alternating-phase level over the common-phase level attains a maximum at about 7 kHz, it is again evident that the noise in this range cannot be predominantly due to a more or less isotropic acoustic field, for in that event the alternating-phase level would continue to increase relative to the other all the way to roughly 9 kHz (see Figs. 3,4). At the same time, if the noise were strictly longitudinal and acoustic, i.e., $\Phi(\bar{k},\omega) \propto \delta(k_1+\omega/c)\delta(k_3)$, the maximum would occur back at 6 kHz. Further, under this assumption the levels would be equal at 3 kHz, rather than at about 4 kHz, as measured. It does not seem excluded, however, that in the frequency range in question, including, in particular, 3 kHz, the predominant noise on both arrays may be acoustic, having a wavenumber spectrum peaked where k_1 is slightly less than ω/c and $|k_3| << k_1$, i.e., peaked in the longitudinal direction but with significant magnitude for k_1 somewhat less than ω/c.

The scaling of measured levels with flow speed is also pertinent and will be considered in Section 5.3.

In all, the evidence does not appear to permit a conclusion as to whether the dominant array noise in the neighborhood of 3 kHz is spurious acoustic noise or boundary-layer pressure fluctuations. Hence the measurements place only an upper limit on the latter contributions.

5.2 Wavenumber Filtering by a Single Microphone

In preparation for detailed analysis of the contribution to measured pressure spectra by the turbulent boundary layer, we must consider the specific area-averaging function $|H(\bar{k})|^2$ for the microphones with their particular facial sensitivity distribution (see Section 3).

A measured sensitivity distribution across the diaphgram diameter of a microphone of the subject type has been given by Brüel and Rasmussen (1959, Fig. 14). The sensitivity function has negligible frequency dependence up to 2 kHz, and, though the frequency filter $|F(\omega)|^2$ decreases perceptibly beyond this, the spatial function $S(\bar{x})$ for use in Eq. 4 changes little on up to 4 kHz. The function $S(\bar{x})$ derived from the measured sensitivity distribution with neglect of small phase differences and assumption of circular symmetry is shown in Fig. 15 (Brüel and Rasmussen 1959).

This function, which we now write $S(r/R)$ with argument (r/R) defined as distance from the element center in units of the sensitive radius ($R \approx 0.378$ in.), can be closely approximated by a function of the form

$$S(r/R)/S(0) = B[1-\beta J_o(\alpha r/R)] \qquad (0<r<R) , \tag{14}$$

with

$$B=0.198,\ \alpha=2.96,\ \beta=-4.06; \tag{15}$$

the latter function is also shown in Fig. 15. Form (14) permits the quadrature of Eq. 4 to be performed to yield the corresponding area-averaging function, written as $|H(\bar{k})|^2 \equiv |H(kR)|^2$, where (Chase 1969)

$$H(z) = \frac{z[1-\beta J_o(\alpha)]J_1(z)+\alpha\beta J_1(\alpha)J_o(z)-\alpha^2 z^{-1}J_1(z)}{(z^2-\alpha^2)[1/2-(\beta/\alpha)J_1(\alpha)]} . \tag{16}$$

In general, as $kR\to\infty$, the least upper bound on $|H(kR)|^2$ decreases as $(kR)^{-3}$ if $S(r/R)$ is discontinuous at $r=R$ [i.e., $S(1)\neq 0$] and as $(kR)^{-5}$ if $S(1)=0$ but the first derivative $S'(r/R)$ is discontinuous [i.e., $S'(1)\neq 0$]. The parameter values (15) satisfy the latter conditions, and (16) yields in this case

$$|H(kR)|^2 \to 2c_o(kR)^{-5}\cos^2(kR-\pi/4) \ , \qquad (17)$$

where

$$c_o = \frac{4\alpha^2\beta^2 J_1^2(\alpha)}{\pi[1-2(\beta/\alpha)J_1(\alpha)]^2} \simeq 5.93 \ ,$$

for $kR>>\alpha$ and $kR>>1$. Though the approximation given by (14) and (15) to the measured sensitivity is generally good, as shown by Fig. 15, it has limited validity with regard to the small-scale variation of the true sensitivity near the element periphery. Accordingly, because of the sensitivity of $H(\bar{k})$ to this variation at large kR, beyond some maximum kR we should not use (16) and (15), or the limiting form (17), except for order-of-magnitude considerations; this safe maximum kR, however, will be large compared to π.

The area-averaging function $|H(kR)|^2$ for the microphone, as approximated by (16) and (15), is shown in Fig. 16 along with the result in Eq. 9 that would apply if the facial sensitivity were uniform. The difference is evidently consequential, the actual lobes being much wider and the rate of decrease from lobe to lobe more rapid. There is no possible choice of a constant

effective radius in a wavenumber filter corresponding to uniform facial sensitivity that can yield this second property; the actual microphone discriminates more effectively against higher wavenumbers.

According to Fig. 16, the level of $|H(\bar{k})|^2$ for the non-uniform facial sensitivity is given at the first two major lobes $k_1=\pi/d$, $3\pi/d$ of the alternating-phase array (for $k_3=0$) by -0.7 dB and -7.1 dB, respectively; thus in contrast to Fig. 2a for uniform sensitivity, in the configuration used the second major lobe is not very well suppressed by the microphone response.

5.3 Estimates Concerning the Low-Wavenumber Boundary-Layer Contribution to Pressure Spectra

So far as the major lobe of $|H(kR)|^2$ is concerned, for kR up to where 10 log $|H(kR)|^2 \simeq -20$ dB, as seen from Fig. 16, the averaging is rather well approximated by the function (9) for the uniform case, provided the effective radius is taken as $R_e=\lambda R$ with $\lambda \simeq 0.72$ (and R=0.378 in.).

We may thus approximate the low-wavenumber contribution, say $\Phi_{M\_}(\omega)$, to the single-microphone spectrum $\Phi_M(\omega)$ of Eq. 5 as

$$\Phi_{M\_}(\omega) \simeq 2\pi \int_0^{\sim \pi/R_e} dk\, k[2J_1(kR_e)/kR_e]^2 \hat{\Phi}(k,\omega) \ , \qquad (18)$$

where $\hat{\Phi}(k,\omega)$ represents the average of $\Phi(\bar{k},\omega)$ over the angle of $\bar{k}$ and the upper limit is chosen to include just the low-k domain where the area-averaging function is large. If the wavenumber spectrum $\hat{\Phi}(k,\omega)$ is roughly constant in the pertinent domain, say equal to $\hat{\Phi}_{\_}(\omega)$, (18) becomes

$$\Phi_{M-}(\omega) \simeq 4\pi R_e^{-2} \hat{\Phi}_-(\omega) \ ; \tag{19}$$

for nonconstant $\hat{\Phi}(k,\omega)$, Eq. 19 may be regarded as defining an average $\hat{\Phi}_-(\omega)$ for the low-k region.

With regard now to the low-wavenumber contribution to the array spectra, say $\Phi_{A-}(\omega)$, we tentatively suppose that $\Phi(\bar{k},\omega)$ remains roughly constant over the width ($\sim\pi/2d$) in k_1 of each major array lobe; except for the possible radiative boundary-layer contribution from wavenumbers k near ω/c, this condition appears highly likely since $\pi/2d << \delta_*^{-1}$. Then from Eqs. 6 and 8 we obtain

$$\Phi_{A-}(\omega) \simeq \sum_m \Phi_{m-}(\omega) \ ; \tag{20a}$$

$$\Phi_{m-}(\omega) \simeq (\pi/2d) \int_{-\infty}^{\infty} dk_3 \left[2J_1((k_m^2+k_3^2)^{1/2} R_e)/(k_m^2+k_3^2)^{1/2} R_e\right]^2 \Phi(k_m,k_3,\omega) \ , \tag{20b}$$

where k_m denotes the wavenumbers of major lobes, i.e.,

$$k_m = \begin{cases} (2m+1)\pi/d, & \text{alternating phase} \\ 2m\pi/d, & \text{common phase} \ , \end{cases}$$

and the sum runs over those small integers (positive, negative, and zero) corresponding to major lobes that may contribute appreciably. If the wavenumber spectrum $\Phi(k_m,k_3,\omega)$ is roughly independent of k_3 in the domain where the integrand may be appreciable, say equal to $\tilde{\Phi}_m(\omega)$, Eq. 20b becomes

$$\Phi_{m-}(\omega) \simeq 2\pi(dR_e)^{-1}(k_m R_e)^{-2} S_1(2k_m R_e)\tilde{\Phi}_m(\omega) \ , \qquad (21)$$

where S_1 denotes a Struve function; more generally, like Eq. 19, this equation defines average values $\tilde{\Phi}_m(\omega)$ of $\Phi(k_m,k_3,\omega)$. ($\tilde{\Phi}_m$ for given m, we note, is not identical for the two types of array.) From (19) and (21) the ratio of the m-th lobe part of the array spectrum to the single-microphone spectrum may be written

$$\Phi_{m-}(\omega)/\Phi_{M-}(\omega) \simeq (2\pi^2)^{-1} N_m^{-2}(d/R_e) S_1(2\pi N_m R_e/d)[\tilde{\Phi}_m(\omega)/\hat{\Phi}_-(\omega)] \ , \qquad (22)$$

where

$$N_m = \begin{cases} 2m+1, \text{ alternating phase} \\ 2m, \quad \text{common phase, } m \neq 0 \ ; \end{cases}$$

for the special instance of common phase, m=0 lobe,

$$\Phi_{o-}(\omega)/\Phi_{M-}(\omega) \simeq (4/3\pi)(R_e/d)[\tilde{\Phi}_o(\omega)/\hat{\Phi}_-(\omega)] \ . \qquad (22b)$$

Including in the sum (20a) the major lobes $k_m = \pm\pi/d, \pm 3\pi/d$ for the alternating-phase array and $k_m = 0, \pm 2\pi/d, \pm 4\pi/d$ for the common phase array, and inserting in (22) numerical values for the present measurements, we obtain

$$\Phi_{A-}(\omega)/\Phi_{M-}(\omega) \simeq \begin{cases} [0.183\tilde{\Phi}_o(\omega) + 0.038\tilde{\Phi}_1(\omega)]/\hat{\Phi}_-(\omega), \\ \qquad\qquad \text{alternating phase} \\ [0.109\tilde{\Phi}_o(\omega) + 0.105\tilde{\Phi}_1(\omega) + 0.010\tilde{\Phi}_2(\omega)]/\hat{\Phi}_-(\omega) \ , \\ \qquad\qquad \text{common phase} \ , \end{cases} \qquad (23)$$

where we have assumed $\tilde{\Phi}_m$ independent of the sign of k_m, as appropriate provided $k_m \ll \omega/U_\infty$. Assuming that the wavenumber spectrum $\Phi(\bar{k},\omega)$ is roughly independent of $\bar{k}$ over all the pertinent domains, so that $\tilde{\Phi}_m(\omega) \simeq \hat{\Phi}_-(\omega) \simeq \Phi(\bar{k},\omega)$, Eq. 23 yields

$$10 \log[\Phi_{A-}(\omega)/\Phi_{M-}(\omega)] \simeq \begin{cases} -6.6 \text{ dB, alternating phase} \\ -6.5 \text{ dB, common phase .} \end{cases} \quad (24)$$

Thus the low-wavenumber boundary-layer contribution to the array spectra is estimated, on assumption of constant $\Phi(\bar{k},\omega)$, to lie below the single-microphone spectra by about 6.5 dB for both arrays (at all speeds). If a measured array spectrum is dominated by this boundary-layer contribution rather than by spurious noise, we should therefore expect that the corresponding single-microphone spectrum would exceed it by about 6.5 dB or more (more if the single-microphone spectrum contains appreciable spurious noise).* The measured spectra in the neighborhood of 3 kHz satisfy this condition and are thus not inconsistent with domination of array spectra by the boundary-layer contribution. Since the measured spectra for the common-phase array exceed those for the alternating-phase array in this frequency range, result (24) would imply that the former spectra are dominated by spurious noise; since the differences are only a few dB, however, the crude assumption of wavenumber-independent $\Phi(\bar{k},\omega)$ entailed in result (24) renders such a conclusion uncertain.

*It will be indicated in Section 5.4 that the high-wavenumber, convective boundary-layer contribution to spectra is not dominant at frequencies $\gtrsim$1.5 kHz.

The assumption of wavenumber independence is of doubtful validity except in the domain where $|k| \gtrsim 1/2\delta^*$ as well as $k_1 << \omega/U_\infty$, and may not apply even under these conditions.

Still assuming wavenumber-independent $\Phi(\bar{k},\omega)$ for boundary-layer pressure in the low-wavenumber domain, we can obtain an upper limit on its (frequency-dependent) value $[=\tilde{\Phi}_m(\omega)]$ from Eqs. 19 and 23 in terms of the measured tenth-octave spectrum $4\pi\psi_A(\omega)$ in the vicinity of 3 kHz (Figs. 8, 9, 10); explicitly we have the relation

$$\Phi(\bar{k},\omega) \lesssim 0.031 \text{ in.}^2 \times \frac{4\pi\Psi_A(\omega)}{\omega/2\pi} \tag{25}$$

Stated in terms of the corresponding contribution $\Phi_-(\omega)$ to the frequency spectrum of pressure on an element with uniform facial sensitivity and arbitrary radius R_o, by the equivalent of Eq. 19 this relation becomes

$$\Phi_-(\omega) \lesssim 0.39 \text{ in.}^2 \times R_o^{-2} \frac{4\pi\Psi_A(\omega)}{\omega/2\pi} \tag{26}$$

Precisely at 3 kHz, for example, Figs. 8, 9, 10, respectively, for $\omega\delta^*/U_\infty \approx 5.0$, 6.2, 8.0, yield by use of (25) $10 \log \Phi(\bar{k},\omega) < -84$, -87, -96 dB re 1 μbar^2-in.^{2}-sec. The admixture of spurious noise may be smaller, however, at slightly higher frequencies; the deep dip at 3.7 kHz for 40 ft/sec in Fig. 10, for example, where $\omega\delta^*/U_\infty \approx 9.8$, yields $10 \log \Phi(\bar{k},\omega) = -103$ dB re 1 μbar^2-in.^{2}-sec.

The upper limit on $\Phi(\bar{k},\omega)$ can be generalized to values of δ^* and U_∞ other than those of the measurements by a suitably consistent assumption concerning the scaling of $\Phi(\bar{k},\omega)$. More

generally, with reference to boundary-layer pressure, including both low-wavenumber and convective contributions (the latter to be considered below in Section 5.4), we may profitably examine the scaling of the measured spectra with flow speed.

The smooth-wall boundary-layer pressure spectrum measured by a single microphone, with radius R permitted to vary but with facial sensitivity distribution fixed, must have the form

$$\Phi_M(\omega) = \rho^2 U_\infty^3 R F_M(\omega R/U_\infty, R/\delta^*) \quad , \tag{27}$$

provided that the frequencies are not so high that the viscous-sublayer thickness parameter ν/v_* also enters, where F_M is a dimensionless function of its dimensionless arguments. Here we neglect the weak Reynolds-number dependence of v_*/U_∞, identifying v_* and U_∞ for scaling purposes. For the fractional-octave spectrum $\psi_M(\omega)$ of (13), from (27) we obtain

$$\psi_M(\omega) = (2\pi)^{-1}(\Delta\omega/\omega) G_M(\omega R/U_\infty, R/\delta^*) \tag{28}$$

where $G_M(x,y) \equiv x F_M(x,y)$. Even if the dependence of G_M on R/δ^* is substantial (and in some domain at least it is not), the dependence of δ^* on U_∞ is sufficiently weak that for the range of U_∞ in the present measurements the dependence of G_M on U_∞ (or N_{Re}) via R/δ^* may be neglected. We define a dimensionless spectrum Δ_M and frequency Ω by

$$\Delta_M = 2\pi(\omega/\Delta\omega)\Psi_M(\omega)/\rho^2 U_\infty^4, \quad \Omega = \omega R/U_\infty.$$

If the measured Ψ_M is due to the boundary layer, by Eq. 28 we then should have $\Delta_M = \Delta_M(\Omega)$, i.e., curves of 10 log Δ_M vs. 10 log Ω should coalesce for different U_∞.

The preceding scaling considerations apply equally to boundary-layer pressure measured by the arrays, apart from entrance of a further variable d/R, which, however, is fixed in the present measurements. We may thus consider the coalescence of the curves 10 log Δ_A vs. 10 log Ω, where, in reference to array measurements, subscript A replaces M.

These dimensionless plots for the measurements at the three speeds are shown in Fig. 17 for the alternating-phase and in Fig. 18 for the common-phase array (note the factor 4π in the ordinate); the measured single-microphone curves are shown in Fig. 17. In this section we examine only a frequency range near 3 kHz (corresponding to 10 logΩ = 11.8, 10.7, 9.8 at U_∞ = 40, 51, 63 ft/sec, respectively), where low-wavenumber boundary-layer pressure may predominate. In the range $4<\Omega<10$ in Fig. 17 for alternating phase, the spectra have roughly constant slope and coalesce well except that the spectrum for 51 ft/sec is somewhat high. It cannot be concluded, however, that boundary-layer noise in fact predominates, since the spurious acoustic noise in the tunnel may scale with speed similarly. Also, in the immediate vicinity of the points corresponding to 3 kHz, where boundary-layer noise is most likely to predominate, the slopes are much steeper and the respective curve segments do not tend to coalesce well.

We consider the range $4<\Omega<10$ in Fig. 17 slightly further despite its questionable relation to boundary-layer pressure. The frequency dependence of the spectra Δ_A there is fairly close to the dependence as ω^{-2} (or ω^{-3} for Φ_A) that would be expected

if the wavenumber spectrum $\Phi(\bar{k},\omega)$ at low k is independent of $\bar{k}$ and of δ^* (e.g., see Chase 1969).* In such case, dimensional considerations require

$$\Phi(\bar{k},\omega) = A_o \rho^2 U_\infty^6 \omega^{-3} \tag{29}$$

and for the corresponding contribution to the frequency spectrum on a uniformly sensitive element of radius R_o

$$\Phi_{-}(\omega) = 4\pi A_o \rho^2 U_\infty^4 \omega^{-1} (\omega R_o / U_\infty)^{-2} \ . \tag{30}$$

Based on the lowest curve (U_∞ = 63 ft/sec) of Fig. 17 in the subject range, we draw a curve, numbered [5] in Fig. 17, with slope such that $\Delta_A \propto \Omega^{-2}$. Adding the 6.6 dB required to refer the result to a single microphone of radius $R_e = 0.72R$, we find from (30) for the value of A_o (or an upper limit thereon)

$$10 \log A_o = -85.4 \ . \tag{31}$$

We may write a slightly modified form of (29) that replaces U_∞ by the more pertinent velocity scale v_* (see Chase 1969):

---

* We emphasize, however, that no development has been advanced to lead us to expect independence of k and δ^* in this domain, and where $\omega/c \lesssim k \lesssim 1/2\delta^*$ we should expect rather that $\Phi(\bar{k},\omega) \propto k^2$.

$$\Phi(\bar{k},\omega) = a_o \rho^2 v_*^6 \omega^{-3} \ ; \qquad (32)$$

the value of a_o implied by agreement with the inferred result (32) at the ratio $v_*/U_\infty \simeq 0.04$ of the present measurement is given by

$$10 \log a_o = -1.4 \ . \qquad (33)$$

Equations 29-31 generalize relations (25), (26) under the further supposition of δ^* independence. As noted above, however, the range in Fig. 18 where $\Delta_A \propto \Omega^{-2}$ does not extend up to values of Ω corresponding to 3 kHz, and the measured spectra near 3 kHz dip steeply to levels below the straight line fitted to Φ_A on assumption of such Ω^{-2} variation. Also, measurements in water for single elements of various sizes by Foxwell (1966), though subject to reservations in the present regard, yield an average dimensionless spectrum $\Phi_M(\omega)/\rho^2 U_\infty^3 R$ that lies somewhat below the upper limit on the low-wavenumber contribution $\Phi_-(\omega)/\rho^2 U_\infty^3 R$ given by Eq. 30 with the value (31) and, in fact, would imply $10 \log a_o \lesssim -3$ in place of the upper limit (33) inferred from the present array measurement.*,** Thus the scaling in (29) and the utility of estimate (31) are questionable.

---

* We assume Foxwell's P(f) is normalized over positive and negative frequencies with f as integration variable.

** Form (34) of the following section, which approximates $\Phi(\bar{k},\omega)$ in the vicinity of the convective ridge, conforms to the scaling (32) in the low-wavenumber domain but is unfounded there. With the coefficient C given the value inferred from the small-element spectrum of Blake (1969) shown in Fig. 7, Eq. (34) would yield $10 \log a_o \simeq -1$. [In terms of A defined in Sec. 5.4, (34) asserts $A_o/A \simeq (2\pi)^{-1} \gamma (v/U_\infty)^2$.]

5.4 The Convective Boundary-Layer Contribution to Pressure Spectra

As indicated by the generally excellent coalescence of dimensionless spectra in Figs. 17 and 18 and by the discussion in Section 4.4, boundary-layer pressure associated with convective wavenumbers ($k_1 \sim \omega/U_c$) predominates in the measured spectra over a substantial frequency range above $\omega R/U_\infty \simeq 1/4$. The upper limit on this range will be estimated here, and the measured array and single-microphone spectra in the range will be studied in the light of present knowledge of $\Phi(\bar{k},\omega)$ in the convective domain.

An array with a sufficiently large number of closely spaced elements would permit more direct and precise exploration of the wavenumber spectral density $\Phi(\bar{k},\omega)$ in the domain of the convective ridge than is readily attained by the usual measurement of cross-spectral densities of pressure between pairs of elements. For the limited array of the present experiment, it is appropriate to compare results with those predicted by a model of $\Phi(\bar{k},\omega)$ in the convective domain that is known to describe the salient properties fairly well. The model considered uniquely satisfies certain kinematic and similarity conditions expected to have approximate validity.

The form referred to is discussed by Chase (1969) and is given by

$$\Phi(\bar{k},\omega)=C^2\rho^2 v_*^3[k_1^2+\gamma^2 k_3^2+(\omega-U_c k_1)^2/v^2+a^2]^{-3/2} , \qquad (34)$$

with $U_c=\eta U_\infty$, $v=sv_*$, $a=(b\delta^*)^{-1}$ and the coefficients a,η,s,γ, and b regarded as substantially constant in the domain considered. For $\omega\delta^*/U_\infty \gtrsim 1$, the term a^2 may be neglected, and the resulting

form is uniquely characterized by the following two properties: [1] It satisfies the similarity condition that the only length scale for boundary-layer pressure in the subject domain is U_∞/ω. [2] The corresponding pressure correlation function is space-time isotropic in a frame convected at velocity U_c (except that streamwise-spanwise spatial anisotropy is permitted in this frame ($\gamma \neq 1$)).* From measurements by Blake (1969) we infer, in the manner discussed by Chase (1969),

$$v/U_c \simeq 0.13,\ \gamma^{-1} \simeq 0.9,\ b \simeq 1.6\ ; \qquad (34a)$$

in the computations below, however, it was assumed that $v/U_c = 0.12$, $\gamma^{-1} = 0.7$. U_c may be identified with the convection velocity defined in the usual way from measurements of longitudinal cross-spectral density (Corcos 1964).

We consider first the single-element spectrum $\Phi_M(\omega)$ predicted from (34) by use of (5):

$$\Phi_M(\omega) = C^2 \rho^2 v_*^3 \iint d^2\bar{k} |H(kR)|^2 [k_1^2 + \gamma^2 k_3^2 + (\omega - U_c k_1)^2/v^2 + a^2]^{-3/2} \ , \qquad (35)$$

*A form similar to (34) but with power -2 instead of -3/2 has been considered by Chandiramani and Blake (1968). Such a form does not satisfy the similarity condition [1] in the appropriate limit (though the resulting normalized cross-spectra do). It also yields normalized cross-spectra whose slopes with respect to the separation variables $\omega\xi_1/U_c$, $\omega\xi_3/U_c$ vanish with $\omega\xi_1/U_c$, unlike form (34) and apparently in conflict with experiment. Likewise, the derived point pressure varies as ω^{-2}, rather than ω^{-1} as in (37).

where H(kR) for the present microphone is given by (16) and (15). For $\omega R/U_c \lesssim 1$, we may set $|H(kR)|^2 \simeq 1$ and obtain the point-microphone spectrum implied by (34)

$$\Phi(\omega) \simeq G_o \rho^2 v_*^4 (\omega^2 + U_c^2/b^2\delta^{*2})^{-1/2} \qquad (36)$$

where $G_o \equiv 2\pi C^2 \gamma^{-1} s$ (and we neglect v^2/U_c^2). For $\omega\delta^*/U_\infty \gtrsim 1$, this assumes the similarity form

$$\Phi(\omega) \simeq G_o \rho^2 v_*^4 \omega^{-1} \ , \qquad (37)$$

discussed by Bradshaw (1967) and Foxwell (1966). Form (37) approximates the measured dependence, which is more closely approximated as $\sim\omega^{-0.7}$, obtained over a wide frequency interval ($0.8 \lesssim \omega\delta^*/U_\infty \lesssim 7$) for a very small element by Blake (1969), as shown in Fig. 7, and also by Hodgson (reported by Bradshaw 1967). For fractional-octave spectra such as plotted in Figs. 8 through 10, or the corresponding dimensionless spectra as plotted in Figs. 17 and 18, Eq. 37 yields a value independent of frequency:

$$\psi_M(\omega) = G_o (2\pi)^{-1} (\Delta\omega/\omega) \rho^2 v_*^4 \quad \text{or} \quad \Delta_M = G_o (v_*/U_\infty)^4 \equiv A \ . \qquad (38)$$

The decrease in the measured Δ_M in Figs. 17 and 18 for frequencies below that for maximum Δ_M is attributed to entrance of dependence on δ^* where $\omega\delta^*/U_\infty \lesssim 1/2$, somewhat as given by (36) for the model (34).*

---

* Eq. 36 may be written as

$$\Phi(\omega)/\rho^2 R U_\infty^3 = A\eta^{-1} (b\delta^*/R)[1 + (b\delta^*/R)^2 \eta^{-2} \Omega^2]^{-1/2} \ ,$$

where $\eta = U_c/U_\infty$, corresponding to a point spectrum constant and proportional to δ^* where $\omega\delta^*/U_\infty << 1$.

The decrease at dimensionless frequencies $\Omega \gtrsim 1$ is due to area averaging ($|H|^2$ in (35)).

In the opposite limit of very large kR, we can satisfactorily estimate the result of (35). First, for $\omega R/U_c \gtrsim 11\pi$, i.e., $\Omega \gtrsim 6\pi$ or $10 \log \Omega \gtrsim 13$, to the extent that (16) still represents the microphone filter at such high kR, we have

$$\Phi_M(\omega) \simeq c_o C^2 \rho^2 v_*^3 R^{-5} \int dk_3 \int dk_1 (k_1^2+k_3^2)^{-5/2} \times [k_1^2+\gamma^2 k_3^2+(\omega-U_c k_1)^2/v^2+a^2]^{-3/2} , \tag{39}$$

where c_o was given at (17). In a rough approximation, becoming valid for $8(v/U_c) \ll 1$, we may further replace the last factor in (39) by a factor $\propto \delta(k_1-\omega/U_c)$ and obtain

$$\Phi_M(\omega) \simeq 4 c_o C^2 \gamma^{-2} \Lambda_{5/2} \rho^2 v_*^3 \, v \, \omega^{-1} (\omega R/U_c)^{-5} ,$$

where

$$\Lambda_{5/2} = \int_o^\infty dz (z^2+1)^{-5/2} (z^2+\gamma^{-2}\alpha_o^2)^{-1} , \quad \alpha_o = [1+(b\omega\delta^*/U_c)^{-2}]^{1/2}$$

$$\simeq (\pi/2) \gamma \alpha_o^{-1} (1+\gamma^{-2}\alpha_o^2)^{-5/2} ,$$

the approximation to $\Lambda_{5/2}$ becoming exact for $\gamma^{-1} \alpha_o \ll 1$. Expressing this final result in terms of the ratio of $\Phi_M(\omega)$ to the point spectrum in (36), we obtain

$$\Phi_M(\omega)/\Phi(\omega) \simeq c_o(1+\gamma^{-2}\alpha_o^2)^{-5/2}(\omega R/U_c)^{-5}$$

$$\simeq 2.1(\omega R/U_c)^{-5} \quad \text{for } \omega\delta^*/U_\infty \gtrsim 1 \ . \tag{40}$$

This ratio represents the asymptotic area correction factor to be applied to the constant Δ_M given in (38) to obtain the Δ_M for comparison with measured results in Fig. 17.

For intermediate values of Ω, the integral (35) could be straightforwardly evaluated numerically. Short of this, we can indicate its rough variation. To this end, we find the result applicable in an imagined limit $\gamma^{-1} \ll 1$, contrary to the actual value (34a) but corresponding to a tractable limit where the last factor in (35) may be considered to be $\propto \delta(k_3)$ except for k_1 near $H(k_1)=0$. At $k_3=0$, the full width in k_1 at half maximum of $\Phi(\bar{k},\omega)$ in (35) is

$$\delta_c k_1 = 1.54\alpha_o(v/U_c)\omega/U_c \sim 0.19\omega/U_c . \tag{41}$$

Hence, except near $H(\omega R/U_c)=0$, we may again regard $\Phi(k_1,0,\omega)$ as $\propto \delta(k_1-\omega/U_c)$ when $0.17\omega/U_c \ll \pi/R$, or $10 \log\Omega \lesssim 5$. In the imagined limit we thus obtain

$$\Phi_M(\omega)/\Phi(\omega) \simeq |H(\omega R/U_c)|^2 \ , \tag{42}$$

which, for assumed U_c/U_∞, is given as a function of Ω from Fig. 16.

We regard the constant G_o or A in Eq. 38 [or C^2 in (34)] as adjustable to fit the measured $\Phi_M(\omega)$ and later compare the value with that given by other measurements. The horizontal line [1] in Fig. 17 corresponds to a dimensionless point spectrum (38) given by

$$10 \log A = -59.6 \ . \qquad (43)$$

Also shown in this figure is the result for Δ_M obtained by applying to this value the asymptotic area-averaging factor (40) (yielding line [3] corresponding to $\Delta_M \propto \Omega^{-4}$ in the figure) and by applying the imaginary limiting form of area-averaging factor (42) for the lowest three lobes of Fig. 16 (curve [2] in the figure), where in both cases we have taken $U_c = 0.7U_\infty$. Exact evaluation of Δ_M from Eq. (35) would yield a function of Ω that would fall somewhat below (perhaps up to ~2 dB below) that given by the unaveraged-in-k_3 function [2] near the lobe peaks (but become equal to it for $\Omega \ll 1$), and would have the valleys between lobes somewhat filled in. Thus the function denoted by [2] represents an "underaveraged" and that by [1] an "overaveraged" approximation to the exact result of (35).

Taking into account the underaveraging, we see in Fig. 17 that the result [2] over its first lobe, i.e., up to $\Omega \approx 4$, agrees rather well with the measured single-microphone result. (The measured results themselves for the three speeds do not very closely coalesce near 10 log $\Omega = 2$, however, an effect which may or may not be real.) This agreement serves to confirm the adequacy of the computed single-microphone filter $|H(kR)|^2$ of Fig. 16 over at least its first lobe.

At higher Ω, the Δ_M (estimated by use of either factor [1] or [2]) falls far below the measured single-microphone spectra, and, in fact, also well below the spectra measured for the alternating-phase array. At sufficiently large $\omega R/U_c$, the single-microphone response will not decline as rapidly as given by approximations (16) or (17), nor hence will Φ_M/Φ for the convective

contribution decline as rapidly as given by (40). Suppose, for example, that the facial sensitivity, though similar to Fig. 15, has an abrupt drop, relative to the central sensitivity, of 0.1 at the microphone edge. The corresponding asymptotic contribution analogous to (40) is then found to be (Chase 1969)

$$\Phi_M(\omega)/\Phi(\omega) \to 0.046(\omega R/U_c)^{-3} \quad . \tag{44}$$

The result of this area-averaging factor applied to the hypothetical point spectrum, with $U_c=0.7U_\infty$, is shown as line [4] in Fig. 17. Though it exceeds the estimate of (40) where $\Omega>5$, it too remains well below all the measured spectra.

We consider the predicted convective-wavenumber part of the boundary-layer pressure spectrum for the array by use of (34) and (16) in (6), resulting in a $\Phi_A(\omega)$ given by (35) with an added factor $|A(\bar{k})|^2$ in the integrand. The integral could be estimated numerically or in crude approximations analogous to (40) and (42). For present purposes, however, it suffices to note that $|A(\bar{k})|^2$, given by Eq. 8, is ≤ 1, whence $\Phi_A(\omega) \leq \Phi_M(\omega)$. (For the actual value of d/R, Φ_A is predicted to lie perhaps up to ~10 dB below Φ_M at the higher Ω.) Since even the single-microphone spectrum Δ_M as estimated above for convective boundary-layer pressure lies well below the measured array spectrum Δ_A, we may thus infer that this estimated contribution to Δ_A would lie at least as far below. Hence, we conclude that beyond 10 log $\Omega \approx 6$ the measured array spectra in Figs. 17 and 18 are probably not dominated by the convective, high-wavenumber contribution to boundary-layer pressure, but by the low-wavenumber contribution or spurious noise.

We may compare with Figs. 17 and 18 a prediction as to how closely Δ_A should approach Δ_M in neighborhoods where

$|A(\omega/U_c,k_3,\omega)|^2$ is near unity (major-lobe peaks). The full width at half maximum of $|A(\bar{k})|^2$ is $\delta_A k_1 \approx 0.456\pi/d$. By (41) and its generalization to $k_3 \neq 0$, we infer that the ratio of the pertinent average width in k_1 of the convective peak in $\Phi(\bar{k},\omega)$ to the width of a major lobe of the array filter is roughly $\omega d/3\pi U_c$. For $U_c/U_\infty \approx 0.75$, this is unity at $\Omega \approx 2$. Therefore, we expect Φ_A/Φ_M will closely approach unity at peaks where $\Omega \lesssim 2$, and less closely as Ω increases. This expectation accords with the results in Figs. 17 and 18. Likewise, at these lower values of Ω the variation of Φ_A is determined mainly by the array filter form rather than by the form of the pressure spectrum $\Phi(\bar{k},\omega)$. To obtain information about the variation of $\Phi(\bar{k},\omega)$ with k_1 over the convective peak ($k_1 \approx \omega/U_c$) at given ω/U_c, we must have a number of elements N and spacing d such that $\omega d/U_c >> 40/N$; at the same time, to sample $\Phi(\bar{k},\omega)$ only at the k_1 for a single major lobe, rather than a sum over two or more lobes, we would require $\omega d/U_c \lesssim 30$.

The point-element value 10 log $\Delta_M \approx -59.6$ given by Eqs. 38 and 43 which, on application of the area-averaging factor, yields a reasonable fit to the measured results for the single-microphone spectra, may be compared with the value inferred more directly from a tangent to the measured spectrum for the smallest element in Fig. 7. By using the level of the latter spectrum in the middle of the range of variation as $\sim\omega^{-0.7}$ to fix the coefficient A in the similarity approximation $\Phi = A\rho^2 U_\infty^4 \omega^{-1}$ (equivalent to Eq. 38), we find 10 log $A \approx -55$, which is about 5 dB higher than the value (43) estimated from the large-element results in Fig.17 .*

*This value inferred from the small-element spectrum measured by Blake (1969) (or the equivalent quantity for variation as $\omega^{-0.7}$) lies about 3 dB above that inferred from the measurements of Bull (1967, Fig. 5).

This discrepancy is not excessive in view of errors associated with the measurements and fitting by the theoretical curves.

6. CONCLUSION

The following conclusions may be drawn from the measurements:

1) The microphone array is a useful device for measuring the wavenumber-frequency spectral density of the wall pressure fluctuations, particularly in the domain of low wavenumbers inaccessible to more usual experimental techniques. The common-phase array is less effective with regard to discrimination against spurious background noise in this measurement than the alternating-phase array but provides a simple means of estimating the background noise spectrum.

2) By measurements with the alternating-phase array, an upper limit has been set on the average low-wavenumber spectral density of boundary-layer pressure fluctuations at given frequency in a high-frequency range, as given by Eqs. 25, 29, and 31. Depending on the scaling law and wavenumber dependence at low wavenumbers, however, this limit may be less restrictive than that implied by certain previous measurements of single-element spectra (Foxwell 1966). Background noise in the tunnel may still have been dominant, and a contribution from high-wavenumber (convective) boundary-layer pressure remained, though it was estimated to be small.

3) In an identifiable domain of dominance by the convective-wavenumber component of boundary-layer pressure, the spectra measured by a single microphone and by arrays show consistency with theoretical predictions based on current knowledge of the

convective-wavenumber spectral density and on a measured facial sensitivity distribution for the microphone.

The results of the measurements suggest the following observations and recommendations.

Considerable uncertainty remains as to whether the low-wavenumber boundary-layer contribution rather than a spurious background contribution to spectra is dominant in the present measurements even at the frequency of maximum discrimination against duct-noise by the alternating-phase array. The primary objective in future experiments should therefore be to reduce still further the spurious background noise. Without modifying the tunnel facility itself, this can be accomplished by increasing the number of array elements. This is a somewhat costly improvement unless the individual microphones are substituted by a specially designed microphone system. A sufficient number of elements would also permit direct measurement of the k_1-variation of the spectral density of boundary-layer pressure over the convective ridge in the frequency range where this convective contribution is dominant.*

Use of an array with an even number of rows parallel to the stream, permitting phases to be alternated in checkerboard fashion, would yield a null in the transverse array-response factor for ductwise background noise ($k_3=0$) at all frequencies. At certain

*If this latter purpose were primary, small sensors (small R/d) should be chosen to extend the frequency range where the convective component predominates.

frequencies, as for the present single-row array, the longitudinal array-response factor would also vanish, yielding a two-fold null. Choice of small center spacing, d_3, in the transverse sense would keep the rate of increase of the transverse response factor small where $|A(\bar{k})|^2 \propto d_3^2$ near $k_3=0$, thereby reducing the acoustic background noise, especially the nearly ductwise component. In order still to maintain high attenuation of the convective pressure contribution by streamwise area averaging without having to operate at higher frequency, one may then consider using rectangular sensors ($L_1 x L_3$) elongated in the streamwise sense. The small width L_3 implied by small d_3 also emphasizes the low-wavenumber boundary-layer contribution relative to the acoustic background by increasing the range of transverse wavenumber acceptance ($|k_3| \lesssim 2\pi/L_3$).*

Choice of relatively small d_3 and hence L_3 is open to the criticism that the resulting range of transverse wavenumbers k_3 accepted exceeds that for the larger sensors of main practical interest. This point seems less serious than might appear, however, since, first, the expected dip in the spectral density of boundary-layer pressure where $k \lesssim 1/2\delta^*$ (but $k \gtrsim \omega/c$) will not seriously affect the noise measured with any sensor having $L_3 << 4\pi\delta^*$ and, second, if the number of streamwise rows is four (or six, etc.) the opportunity exists to partially infer the k_3 dependence of the pressure, and hence extrapolate to somewhat wider sensors, by varying the weighting coefficients assigned to elements in the various transverse positions.

---

*If L_3/L_1 were so small that $\omega L_3/U_\infty \lesssim \pi$ at the useful frequencies, smaller L_3 would probably emphasize the low-wavenumber boundary-layer contribution also relative to the convective contribution.

The longitudinal facial sensitivity of a rectangular sensor should preferably be designed to taper smoothly toward the edges for maximum attenuation of convective (high-wavenumber) pressure.

Use of rectangular sensors has the additional advantage that their wavenumber filters for area averaging are separable into longitudinal and transverse factors, simplifying the theoretical analysis (e.g., see Chase 1969).

We therefore recommend extension of measurements of the present kind to arrays with even-multiple streamwise rows, preferably using closely packed rectangular sensors relatively narrow spanwise, with variable element weights.

There is some advantage in employing a microphone spacing such that the second major lobe ($k_1=3\pi/d$) of the alternating-phase array is more nearly suppressed by microphone area averaging for the particular facial sensitivity distribution of the microphones, in order to confine low-wavenumber contributions largely to the vicinity of a single value of k_1. The consideration of maximum attenuation of convective pressure at an acceptable frequency of operation appears, however, a more important design criterion.

Consideration should be given also to providing steering of the array (Maidanik and Jorgensen 1967) by use of delay lines or by equivalent digital processing of time-referenced individual records. This step would permit, in particular, achieving maximum discrimination against duct noise at any given frequency, rather than only one or a few, with fixed microphone spacing.

REFERENCES

Blake, W.K. 1969 M.I.T. Dept. of Naval Arch. and Engin., Acoustics and Vibration Lab. Rept. No. 70208-1.

Bradshaw, P. 1967 J. Fluid Mech. 30, 241.

Brüel, P.V. and Rasmussen, G. 1959 Bruel & Kjaer Tech. Rev., No.2.

Bull, M.K. 1967 J. Fluid Mech. 28, 719.

Chandiramani, K.L. & Blake, W.K. 1968 Bolt Beranek and Newman Inc. Report No. 1557.

Chandiramani, K.L. 1968 Bolt Beranek and Newman Inc. Report No. 1728.

Chase, D.M. 1969 J. Acoust. Soc. Amer., in publication.

Corcos,G.M. 1963 J. Acoust. Soc. Amer. 35, 192.

Corcos,G.M. 1964 J. Fluid Mech. 18, 353.

Foxwell, J.H. 1966 Admiralty Underwater Weapons Establishment Tech. Note 218/66.

Hinze, J.O. 1959 Turbulence (McGraw-Hill Book Co., Inc.,New York).

Maidanik, G. and Jorgensen, D.W. 1967 J. Acoust. Soc. Amer. 42, 494.

Uberoi, M.S. and Kovasznay, L.S.G. 1953 Quart. Appl. Math. 10, 375.

Willmarth, W.W. & Woodridge, C.E. 1962 J. Fluid Mech. 14, 187.

Wills, J.A.B. 1967 National Physical Laboratory, Teddington, Aero Rept. No. 1224.

CAPTIONS FOR FIGURES

Fig. No.

1. Array wavenumber response for alternating phase (upper) and common phase (lower) with N=4.

2. Combined wavenumber filter vs. k_1 at k_3=0 for array of uniform circular microphones with $3\pi R/d \approx 3.8$: (a) alternating phase, (b) common phase.

3. Measured and calculated response of alternating-phase array for plane-wave calibration signal along duct (corrected for frequency dependence of microphone sensitivity).

4. Calculated response of common-phase array as in Fig. 3.

5. Mean velocity profiles in wind tunnel.

6. Comparison of measured velocity defects with that calculated from Cole's law of the wake.

7. Dimensionless boundary-layer pressure spectra measured by single microphone in present and other experiments.

8. Tenth-octave pressure levels measured by alternating-phase array and by single one-inch microphone at 63 ft/sec.

9. Tenth-octave pressure levels measured by alternating-phase array and by single one-inch microphone at 51 ft/sec.

10. Tenth-octave pressure levels measured by alternating-phase array and by single one-inch microphone at 40 ft/sec.

Fig. No.

11 Tenth-octave pressure levels measured by common-phase array and by single one-inch microphone at 63 ft/sec.

12 Tenth-octave pressure levels measured by common-phase array and by single one-inch microphone at 51 ft/sec.

13 Tenth-octave pressure levels measured by common-phase array and by single one-inch microphone at 40 ft/sec.

14 Difference in noise levels measured by common-phase and alternating-phase arrays and difference computed for longitudinal acoustic noise.

15 Measured facial sensitivity distribution of microphone (Brüel and Rasmussen 1959) and function used to approximate it.

16 Microphone wavenumber filters (1) computed from approximation to measured facial sensitivity of Fig. 15 and (2) given by $[2J_1(kR)/kR]^2$ for uniform sensitivity and same radius.

17 Tenth-octave dimensionless spectra measured by alternating-phase array and by single microphone with related theoretical spectra: [1] $\Delta_M=A=10^{-5.96}$, hypothetical boundary-layer point-pressure spectrum; [2] $\Delta_M=A|H(\omega R/0.7U_\infty)|^2$, convective contribution to boundary-layer spectrum wavenumber-filtered by single microphone (unaveraged in k_3); [3] $\Delta_M=2.1A(\omega R/0.7U_\infty)^{-5}$, convective boundary-layer spectrum wavenumber-filtered by single microphone (limit of large $\omega R/U_\infty$); [4] $\Delta_M = 0.046(\omega R/0.7U_\infty)^{-3}$, filtered convective spectrum for discontinuity of 0.1 in facial

Fig. No.

(17) sensitivity (limit of large $\omega R/U_\infty$); [5] $\Delta_A \propto (\omega R/U_\infty)^{-2}$, fit to lowest measured array spectrum in range $7 \lesssim 10 \log(\omega R/U_\infty) \lesssim 10$.

18 Tenth-octave dimensionless spectra measured by common-phase array.

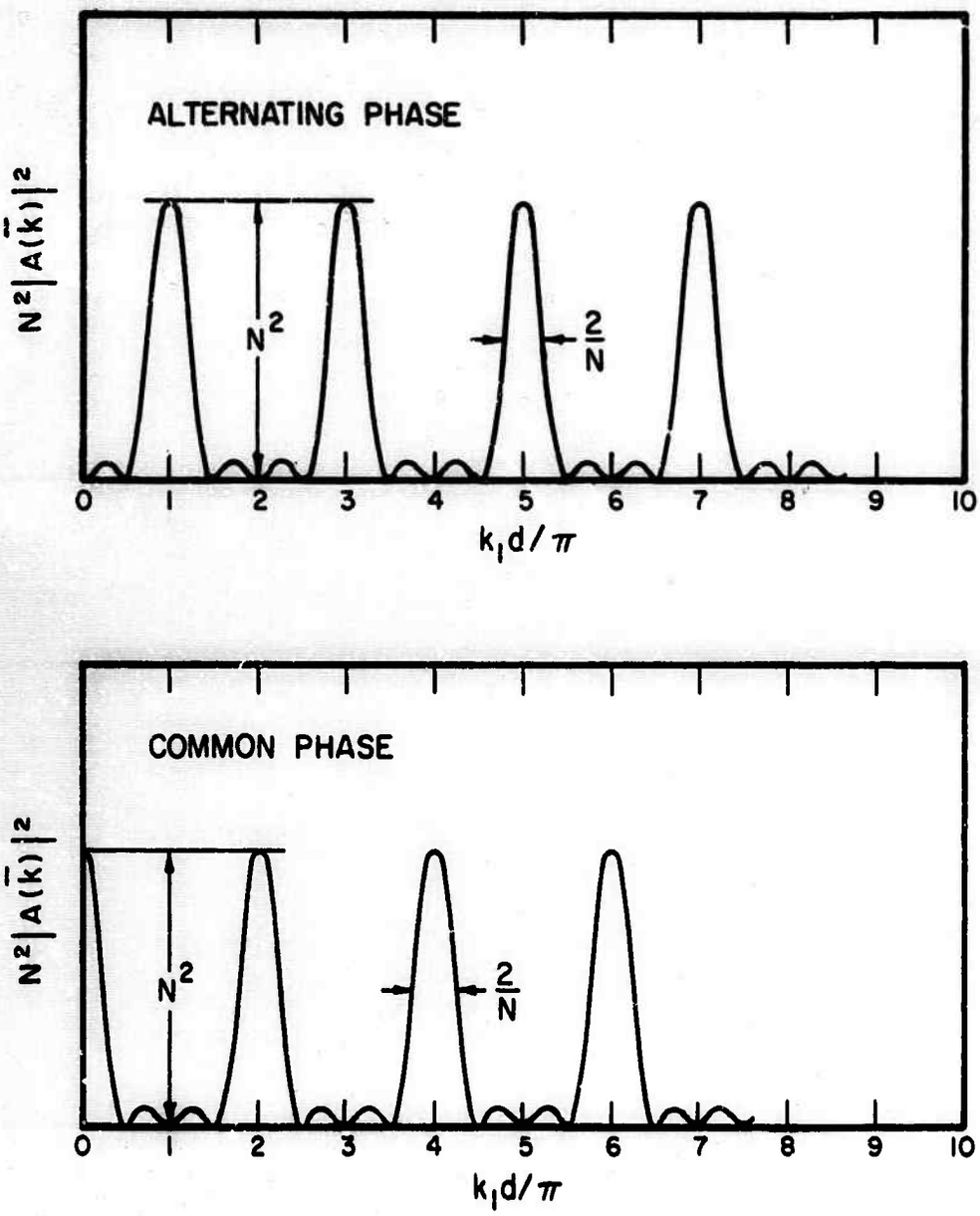
ALTERNATING PHASE
$N^2|A(\bar{k})|^2$
N^2
$\frac{2}{N}$
0 1 2 3 4 5 6 7 8 9 10
$k_1 d/\pi$
COMMON PHASE
$N^2|A(\bar{k})|^2$
N^2
$\frac{2}{N}$
0 1 2 3 4 5 6 7 8 9 10
$k_1 d/\pi$

FIG.1

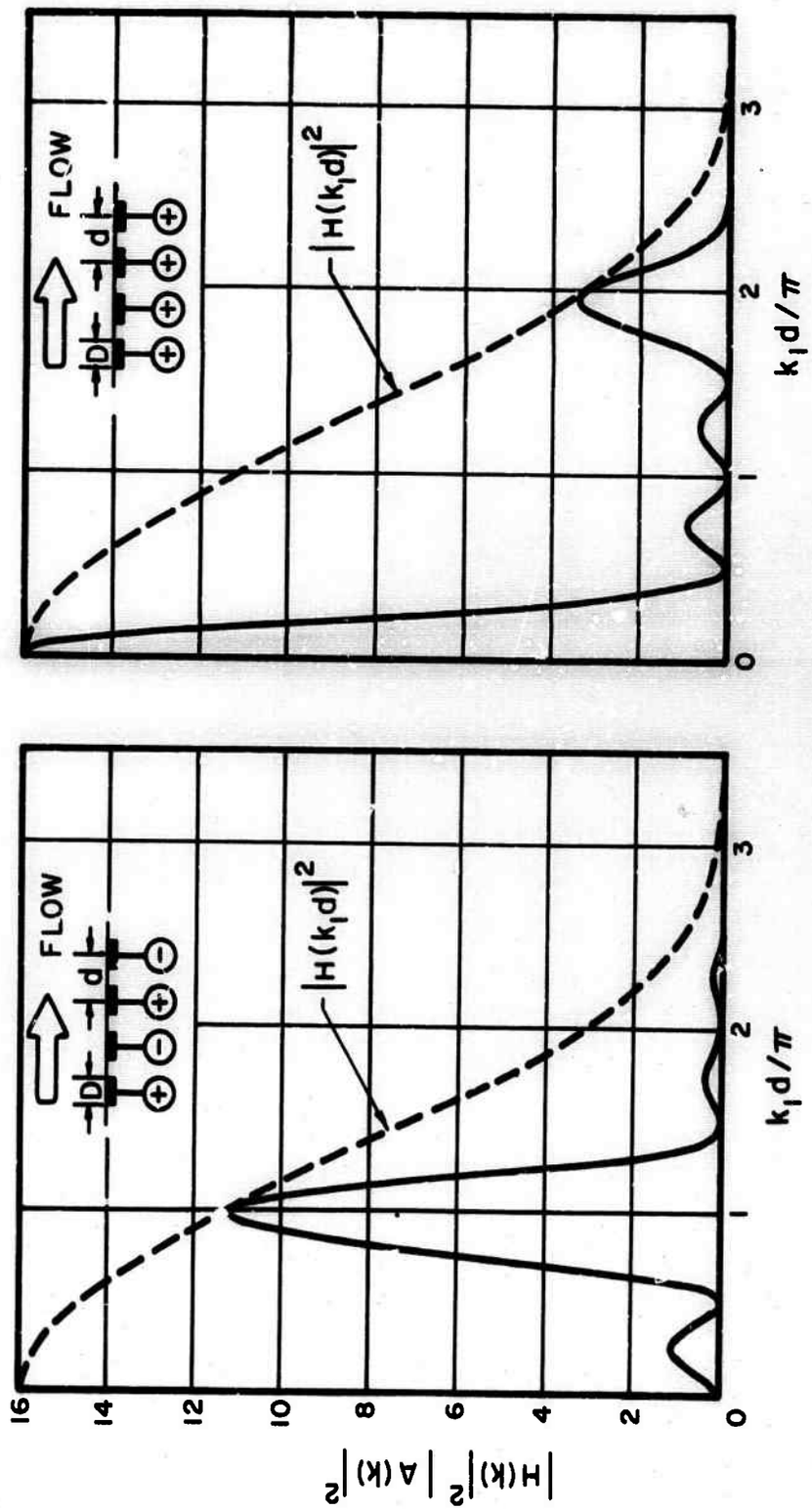
FLOW
D
d
$|H(k_1d)|^2$
k_1d/π
0
1
2
3
FLOW
D
d
$|H(k_1d)|^2$
k_1d/π
0
1
2
3
$|H(k)|^2 |A(k)|^2$
0
2
4
6
8
10
12
14
16

FIG.2

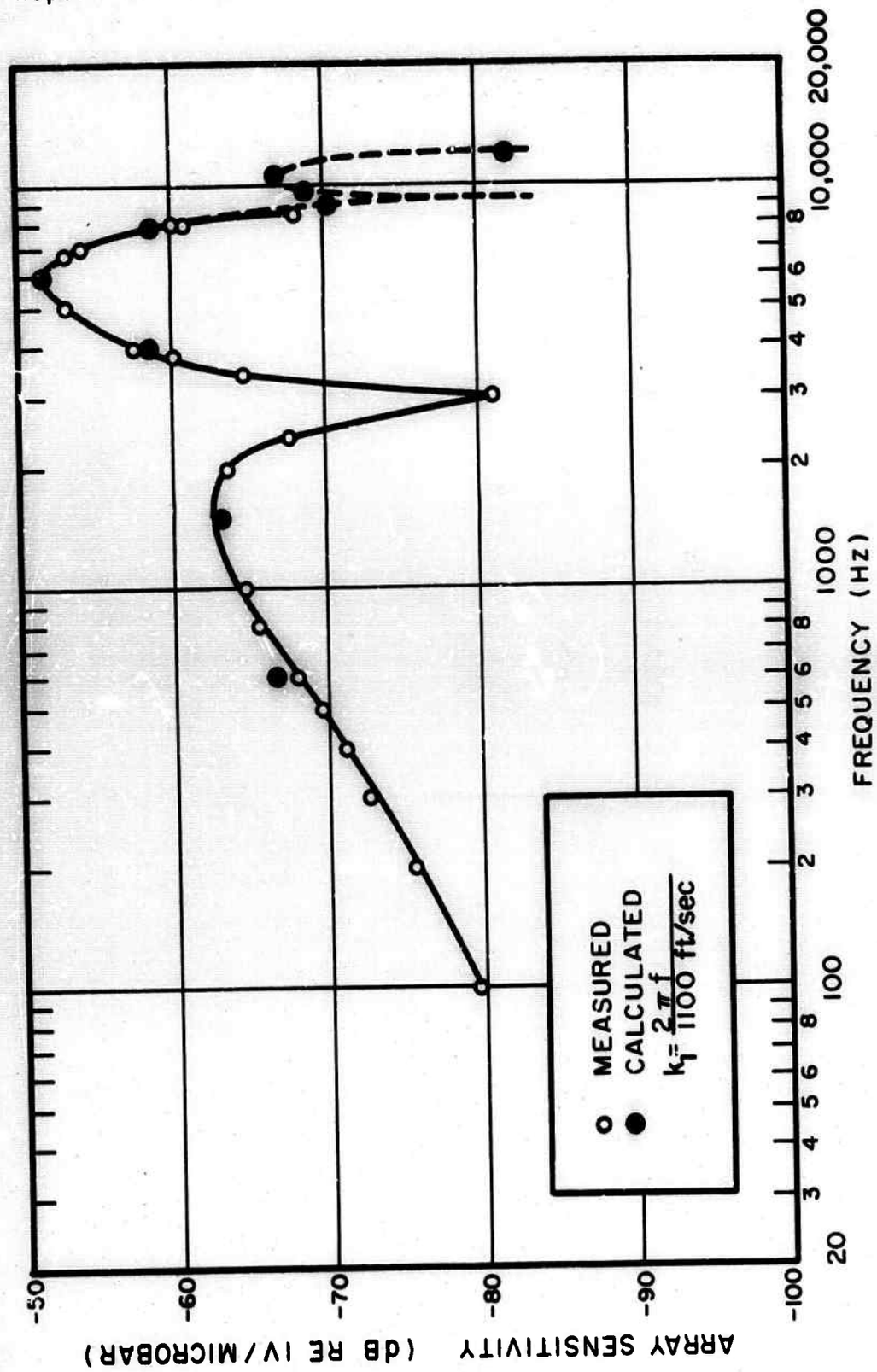
ARRAY SENSITIVITY (dB RE 1V/MICROBAR)
-50
-60
-70
-80
-90
-100
20
3
4
5
6
8
100
2
3
4
5
6
8
1000
2
3
4
5
6
8
10,000
20,000
FREQUENCY (Hz)
MEASURED
CALCULATED
$k_f = \frac{2\pi f}{1100 \text{ ft/sec}}$

FIG. 3

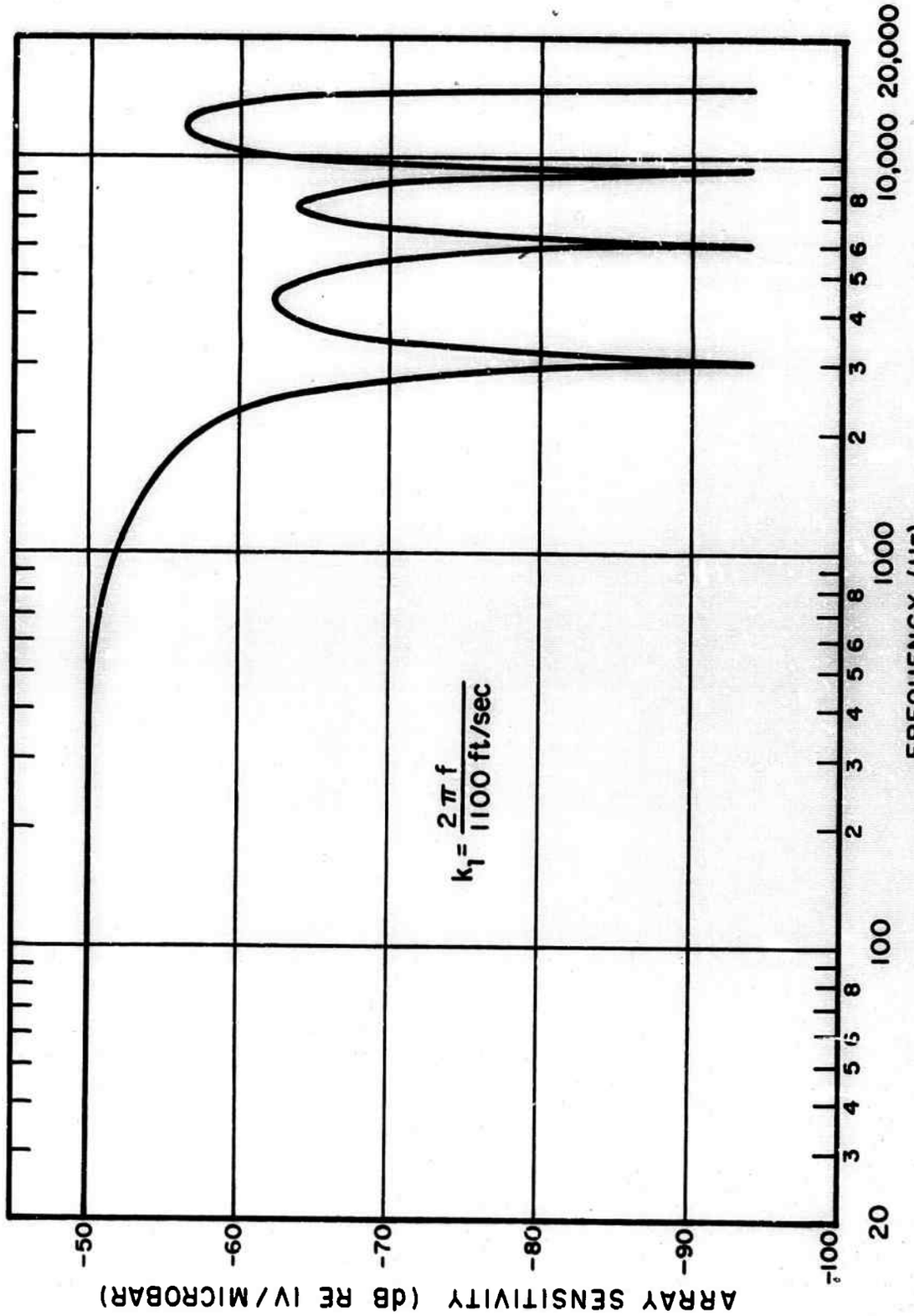
ARRAY SENSITIVITY (dB RE 1V/MICROBAR)
-50
-60
-70
-80
-90
-100
20
100
1000
10,000 20,000
FREQUENCY (Hz)
$k_1 = \frac{2\pi f}{1100 \text{ ft/sec}}$

FIG. 4

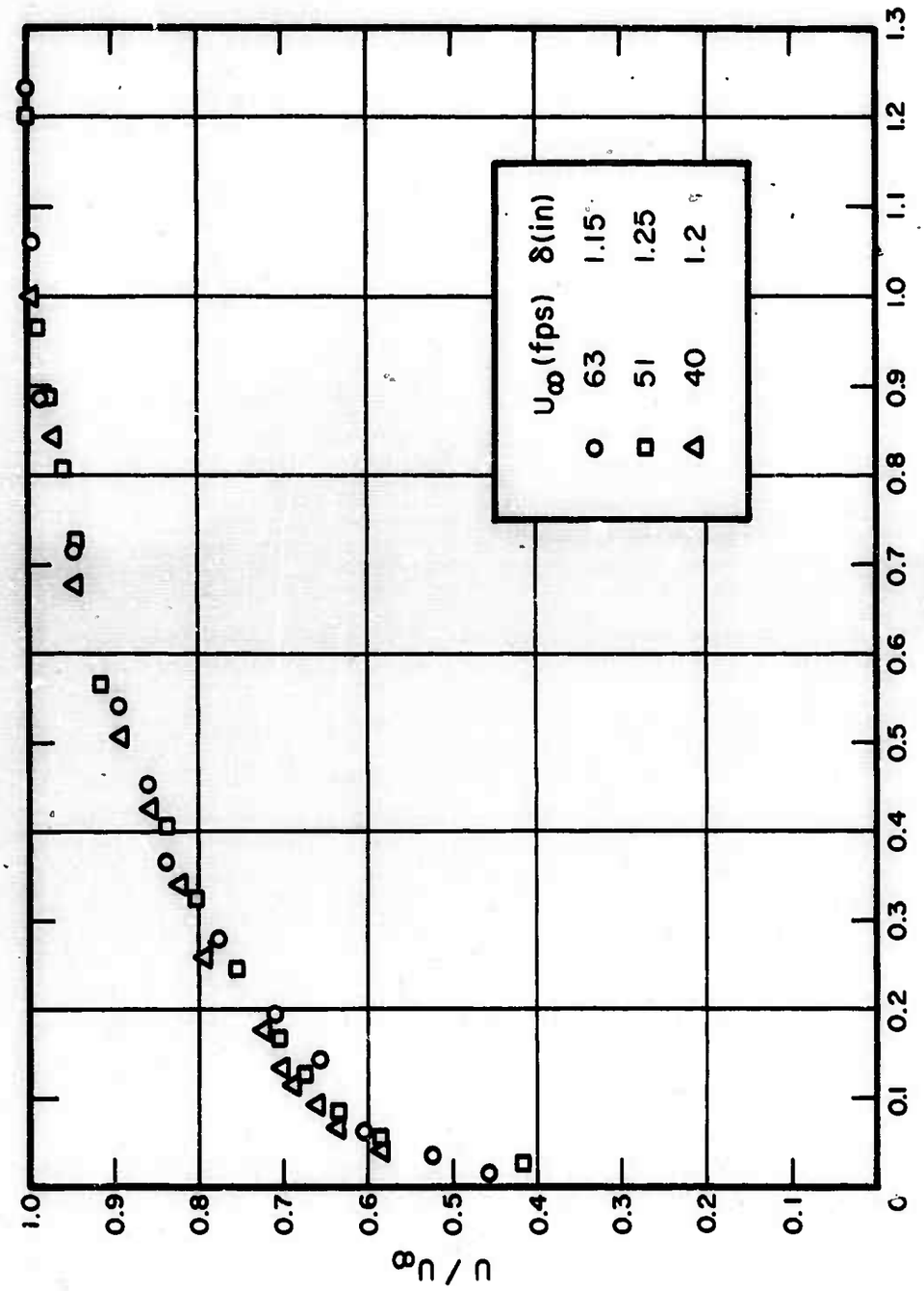
U_∞(fps) δ(in)
63 1.15
51 1.25
40 1.2
u / u_δ
y/δ.99
0
0.1
0.2
0.3
0.4
0.5
0.6
0.7
0.8
0.9
1.0
1.1
1.2
1.3

FIG.5

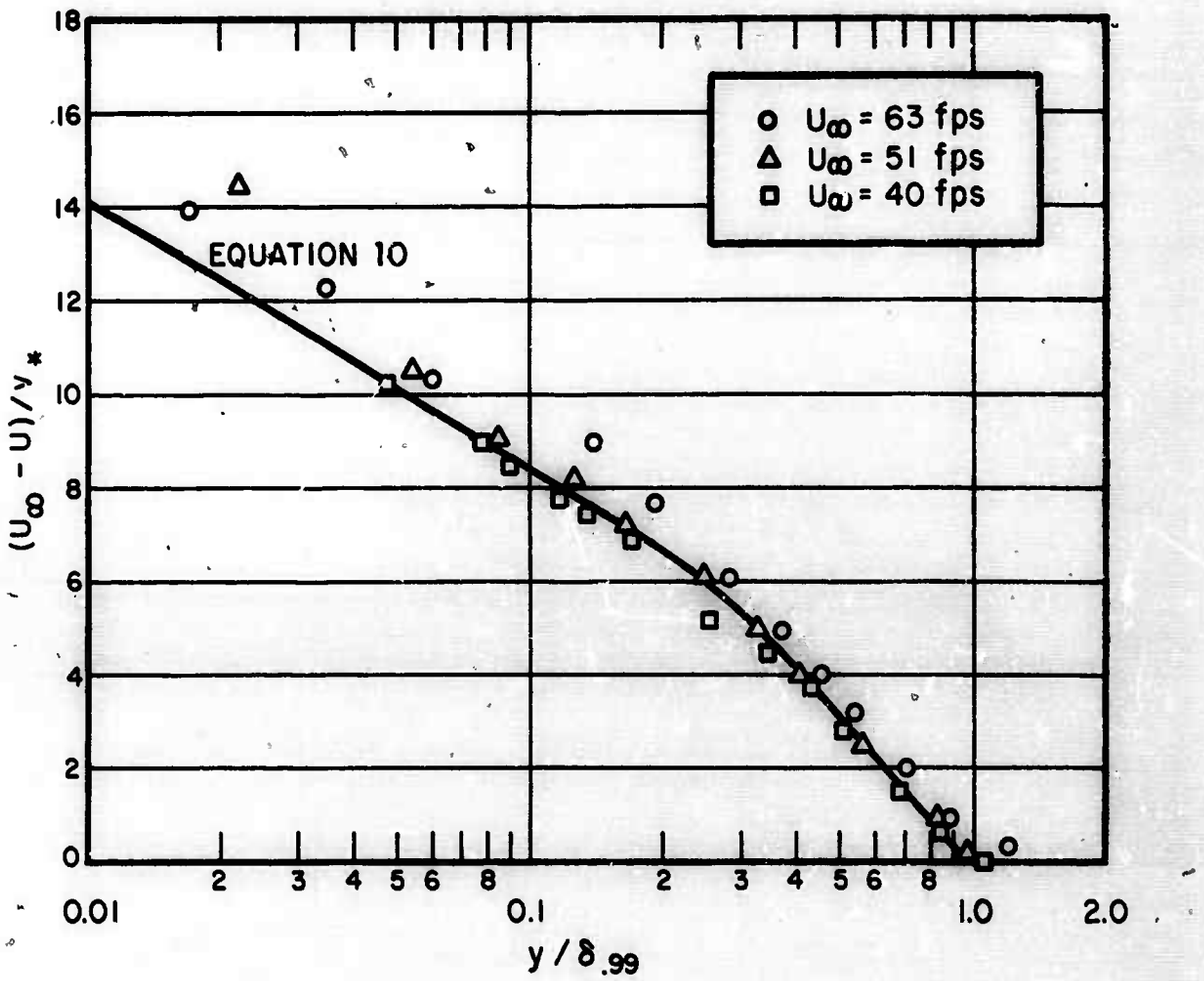
U_∞ = 63 fps
U_∞ = 51 fps
U_∞ = 40 fps
EQUATION 10
$(U_\infty - U)/v_*$
$y/\delta_{.99}$
0.01
0.1
1.0
2.0

FIG.6

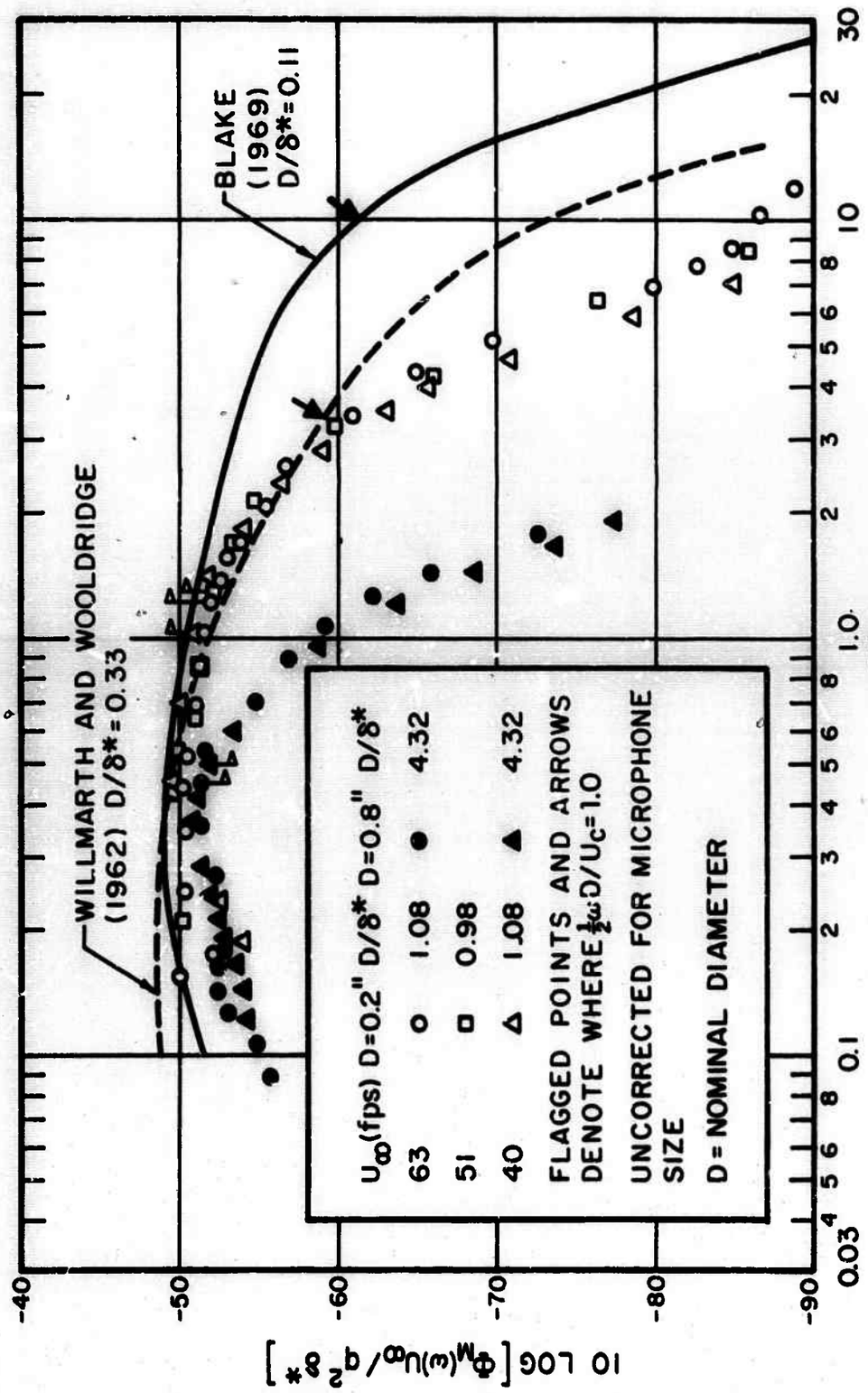
BLAKE (1969) D/δ*=0.11
WILLMARTH AND WOOLDRIDGE (1962) D/δ*=0.33
U_∞(fps) D=0.2" D/δ* D=0.8" D/δ*
63 ○ 1.08 ● 4.32
51 □ 0.98
40 △ 1.08 ▲ 4.32
FLAGGED POINTS AND ARROWS DENOTE WHERE ½ωD/U_c=1.0
UNCORRECTED FOR MICROPHONE SIZE
D= NOMINAL DIAMETER
10 LOG [$\Phi_M(\omega)U_\infty/q^2\delta^*$]
-40
-50
-60
-70
-80
-90
0.03
0.1
1.0
2
3
4
5
6
8
10
30
ωδ*/U_∞

FIG.7

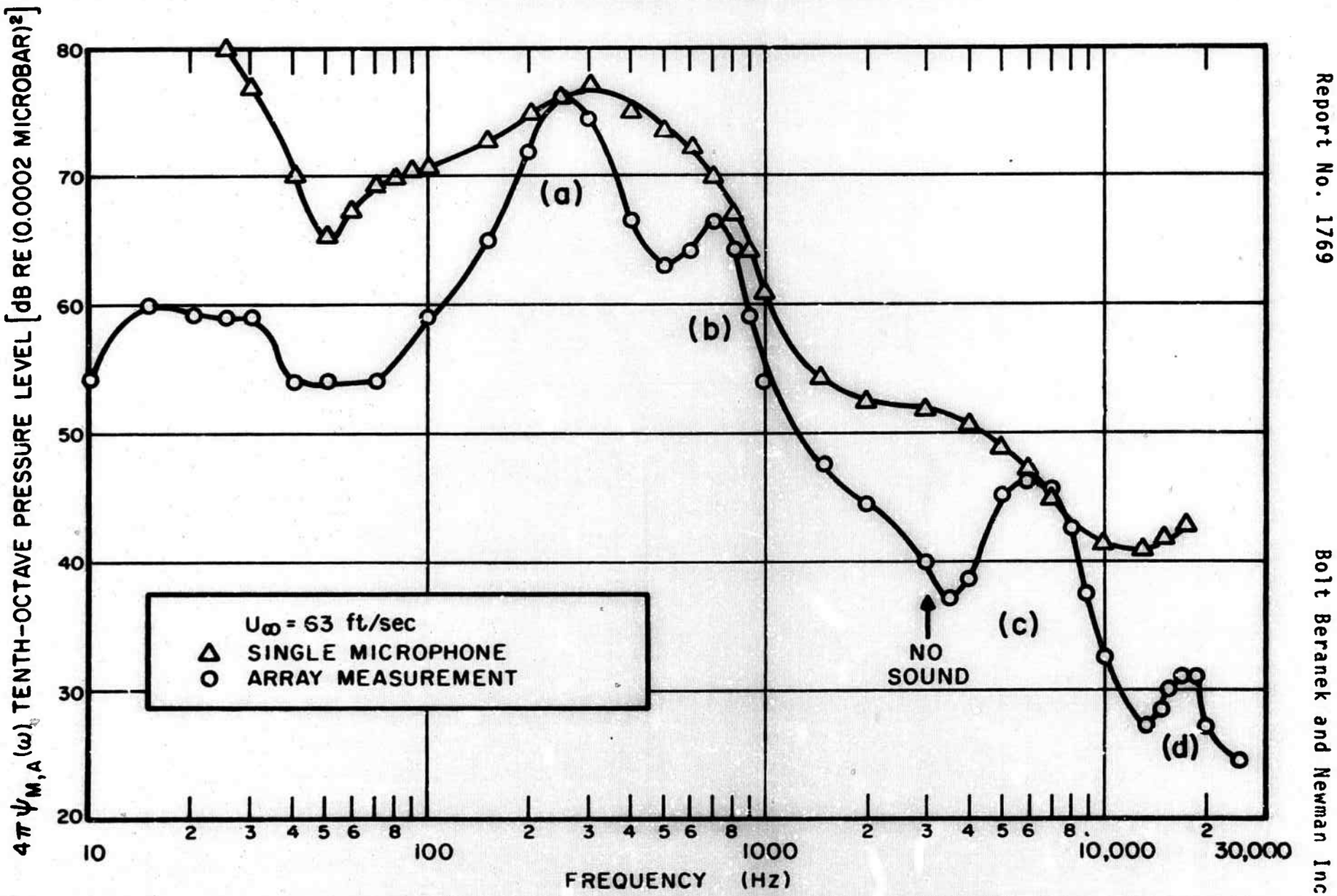
$4\pi\psi_{M,A}(\omega)$, TENTH-OCTAVE PRESSURE LEVEL [dB RE (0.0002 MICROBAR)^2]
80
70
60
50
40
30
20
10
2
3
4
5
6
8
100
1000
10,000
30,000
FREQUENCY (Hz)
U_∞ = 63 ft/sec
SINGLE MICROPHONE
ARRAY MEASUREMENT
(a)
(b)
(c)
(d)
NO SOUND

FIG.8

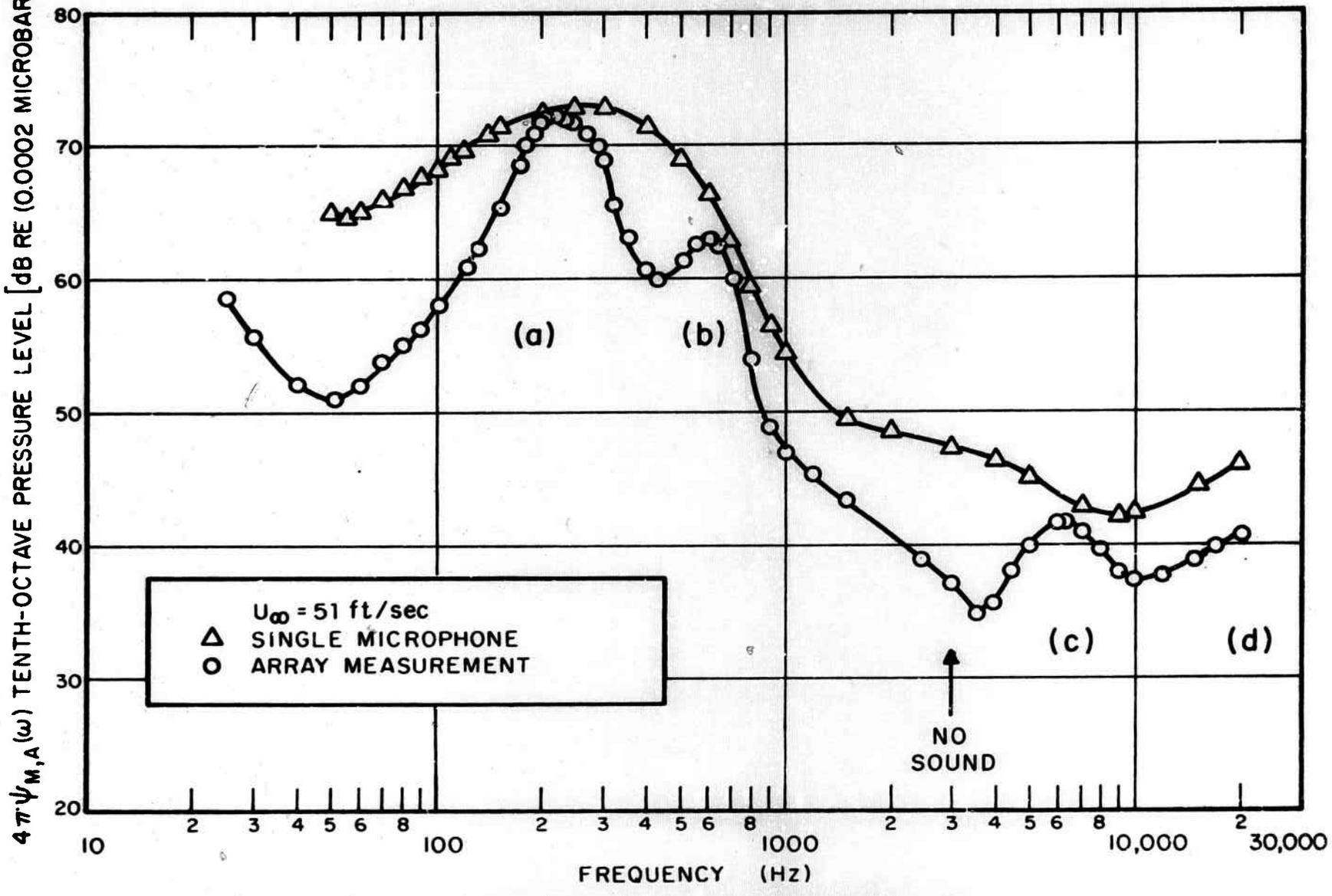
$4\pi\psi_{M,A}(\omega)$ TENTH-OCTAVE PRESSURE LEVEL [dB RE (0.0002 MICROBAR)^2]
80
70
60
50
40
30
20
10
100
1000
10,000
30,000
FREQUENCY (Hz)
U_∞ = 51 ft/sec
SINGLE MICROPHONE
ARRAY MEASUREMENT
(a)
(b)
(c)
(d)
NO SOUND

FIG.9

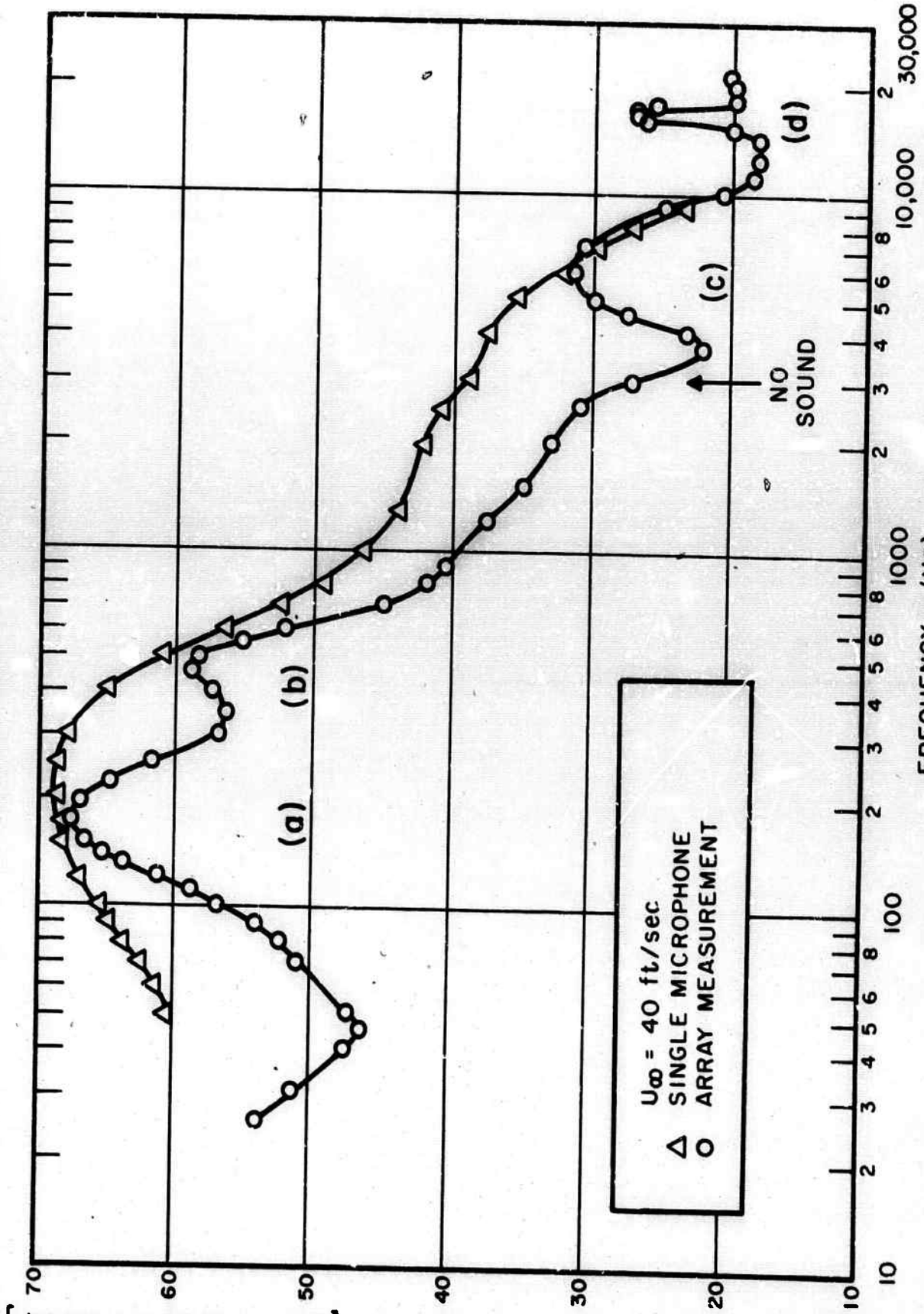
$4\pi\psi_{M,A}(\omega)$ TENTH-OCTAVE PRESSURE LEVEL [dB RE (0.0002 MICROBAR)^2]
70
60
50
40
30
20
10
10
100
1000
10,000
30,000
FREQUENCY (Hz)
(a)
(b)
(c)
(d)
NO SOUND
U_∞ = 40 ft/sec
Δ SINGLE MICROPHONE
O ARRAY MEASUREMENT

FIG. 10

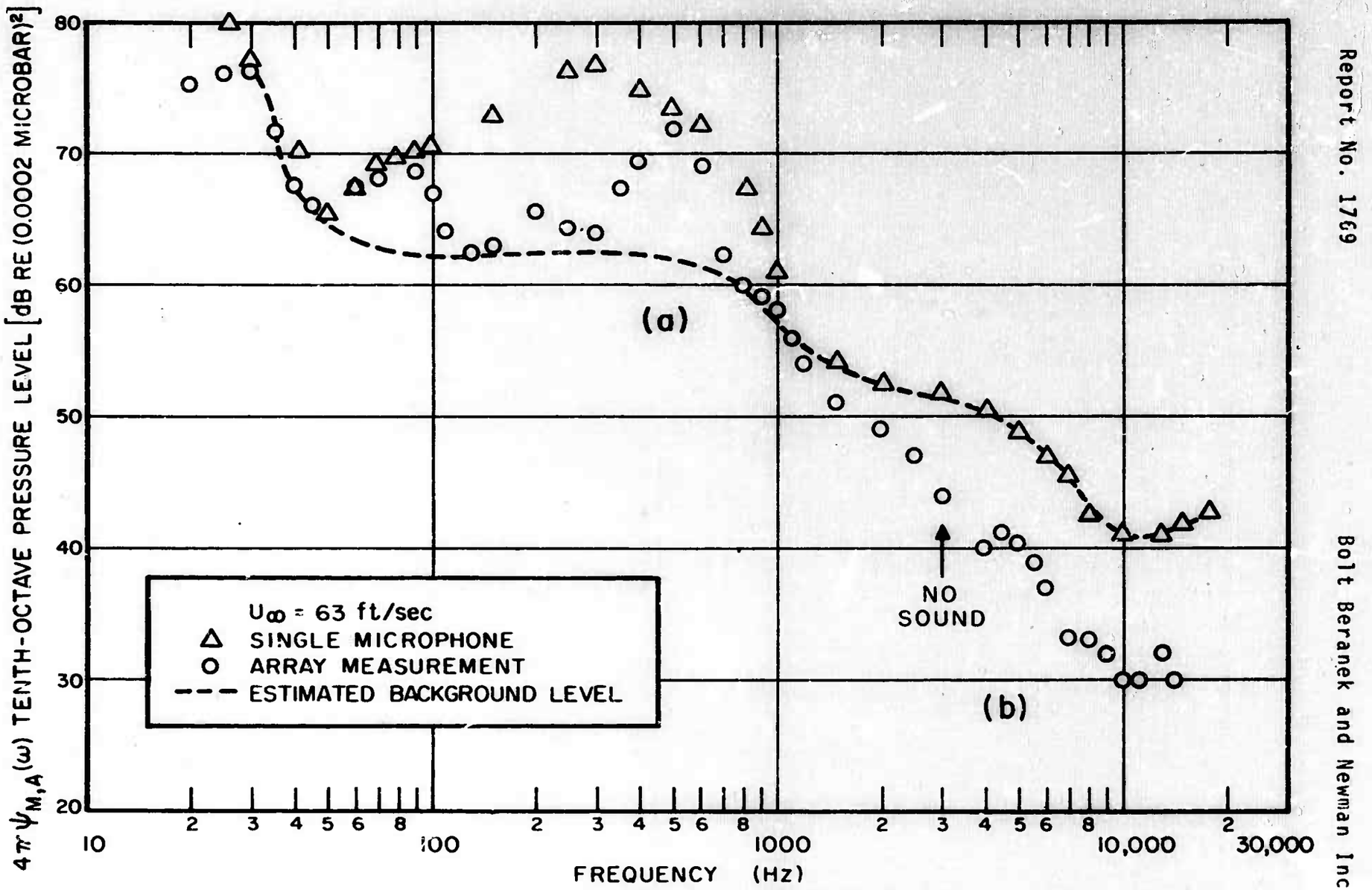
$4\pi\psi_{M,A}(\omega)$ TENTH-OCTAVE PRESSURE LEVEL [dB RE (0.0002 MICROBAR)^2]
80
70
60
50
40
30
20
10
100
1000
10,000
30,000
FREQUENCY (Hz)
(a)
(b)
NO SOUND
U_∞ = 63 ft/sec
SINGLE MICROPHONE
ARRAY MEASUREMENT
ESTIMATED BACKGROUND LEVEL

FIG. 11

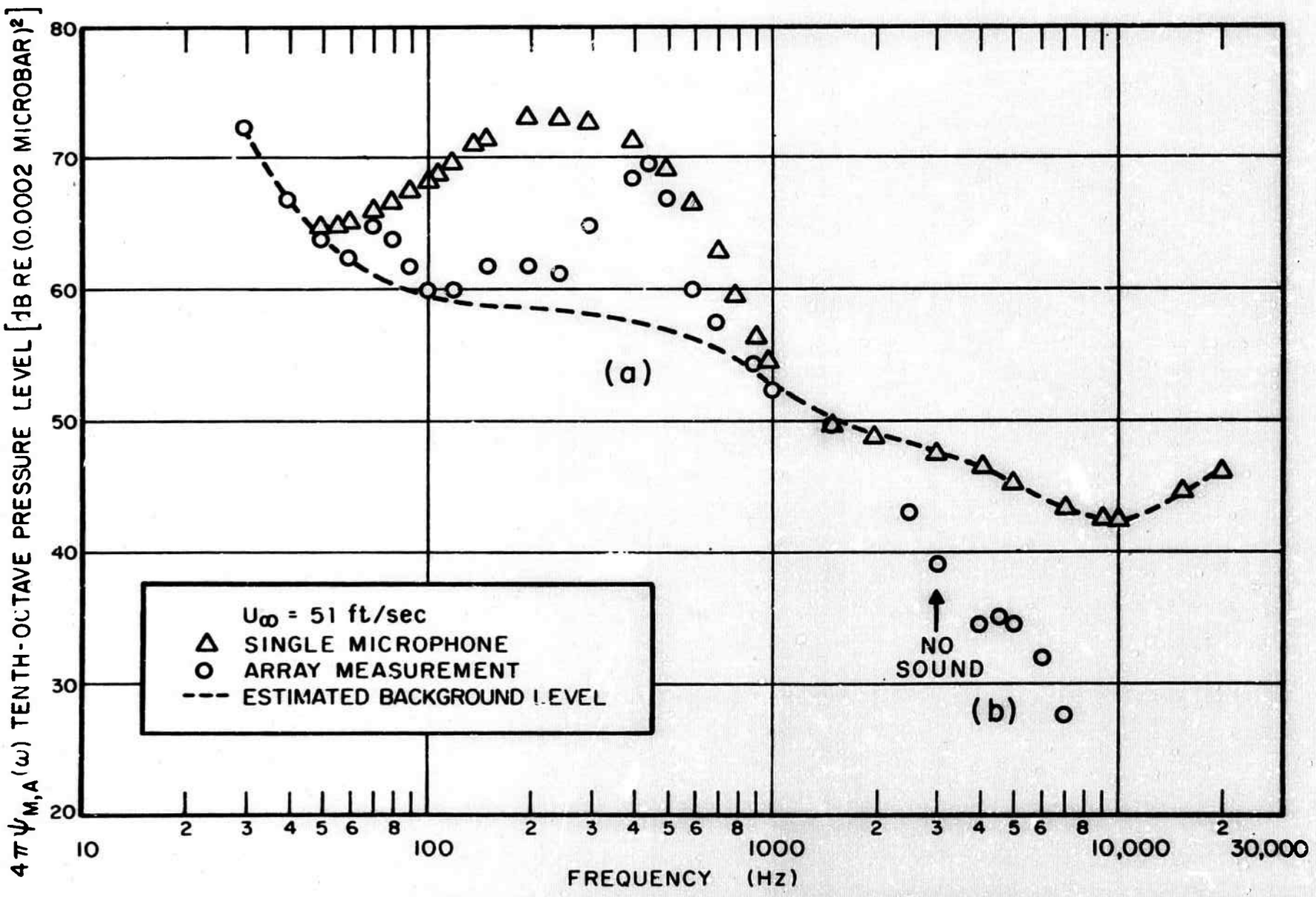
$4\pi\psi_{M,A}(\omega)$ TENTH-OCTAVE PRESSURE LEVEL [dB RE (0.0002 MICROBAR)^2]
80
70
60
50
40
30
20
10
100
1000
10,000
30,000
FREQUENCY (Hz)
U_∞ = 51 ft/sec
SINGLE MICROPHONE
ARRAY MEASUREMENT
ESTIMATED BACKGROUND LEVEL
(a)
(b)
NO SOUND

FIG.12

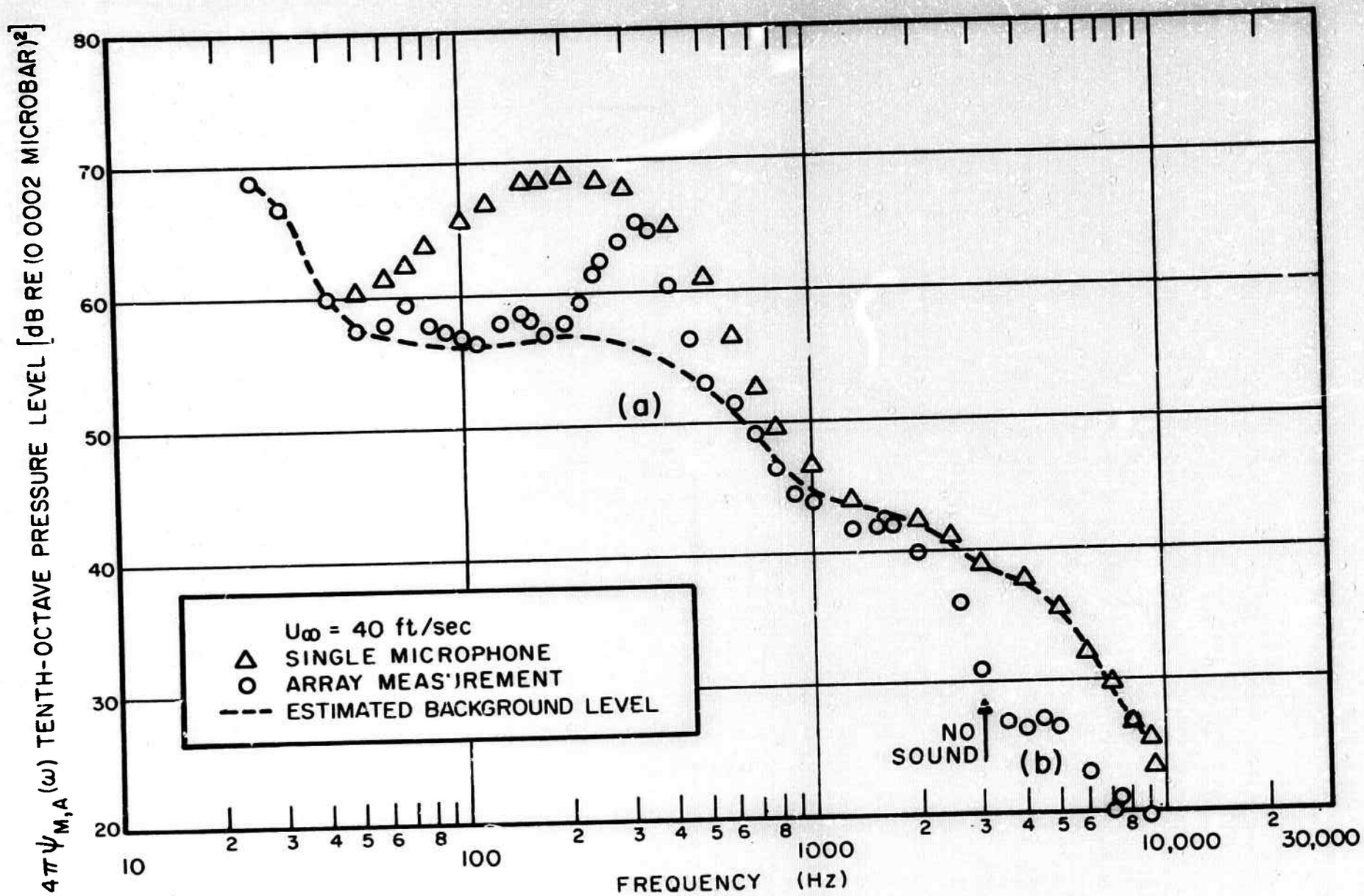
$4\pi\psi_{M,A}(\omega)$ TENTH-OCTAVE PRESSURE LEVEL [dB RE (0.0002 MICROBAR)^2]
80
70
60
50
40
30
20
10
100
1000
10,000
30,000
FREQUENCY (Hz)
(a)
(b)
NO SOUND
U_∞ = 40 ft/sec
SINGLE MICROPHONE
ARRAY MEASUREMENT
ESTIMATED BACKGROUND LEVEL

FIG.13

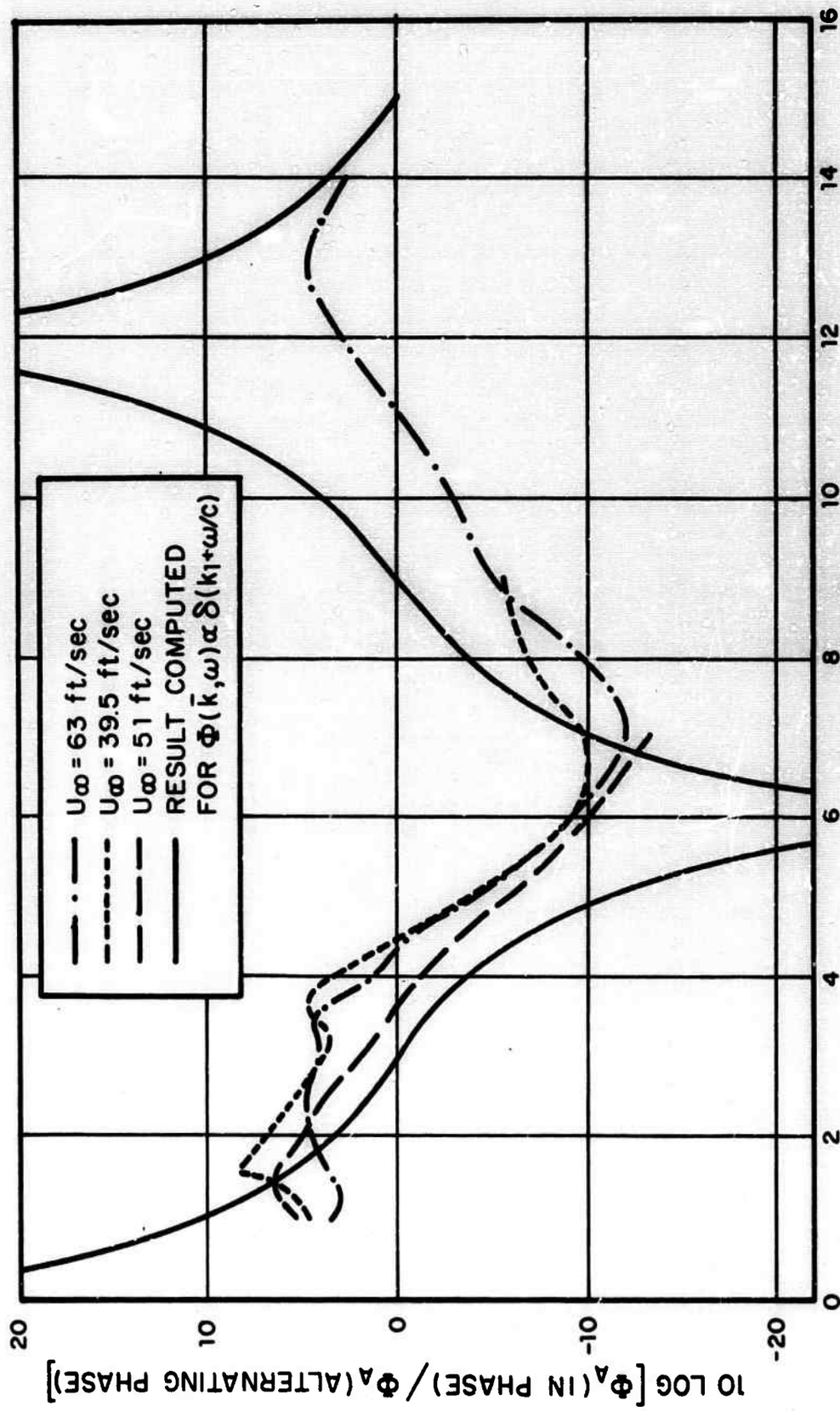
U_∞ = 63 ft/sec
U_∞ = 39.5 ft/sec
U_∞ = 51 ft/sec
RESULT COMPUTED FOR $\Phi(\bar{k},\omega) \propto \delta(k_1+\omega/c)$
FREQUENCY (kHz)
0
2
4
6
8
10
12
14
16
20
10
0
-10
-20
10 LOG [Φ_A(IN PHASE)/ Φ_A(ALTERNATING PHASE)]

FIG.14

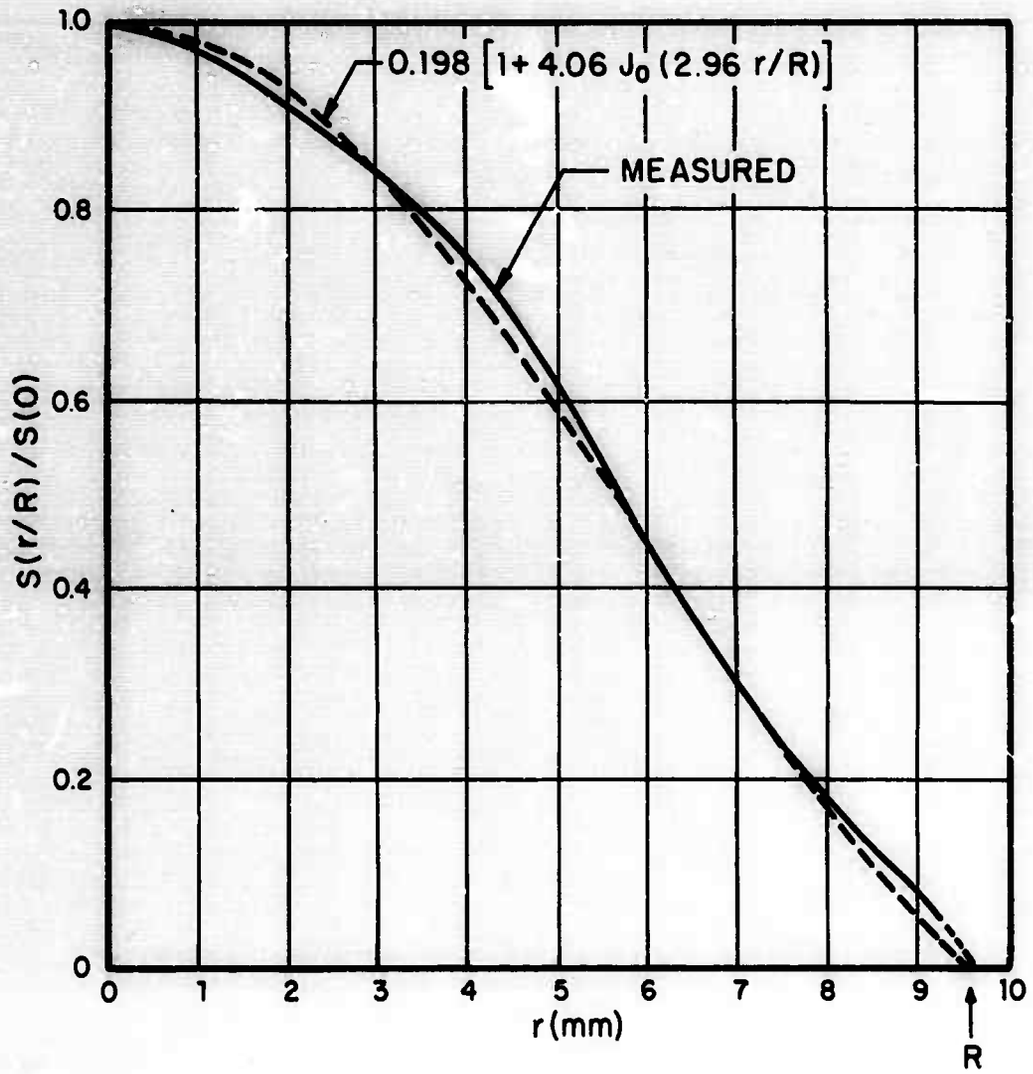
1.0
0.8
0.6
0.4
0.2
0
S(r/R)/S(0)
0.198 [1+ 4.06 J0 (2.96 r/R)]
MEASURED
0 1 2 3 4 5 6 7 8 9 10
r(mm)
R

FIG.15

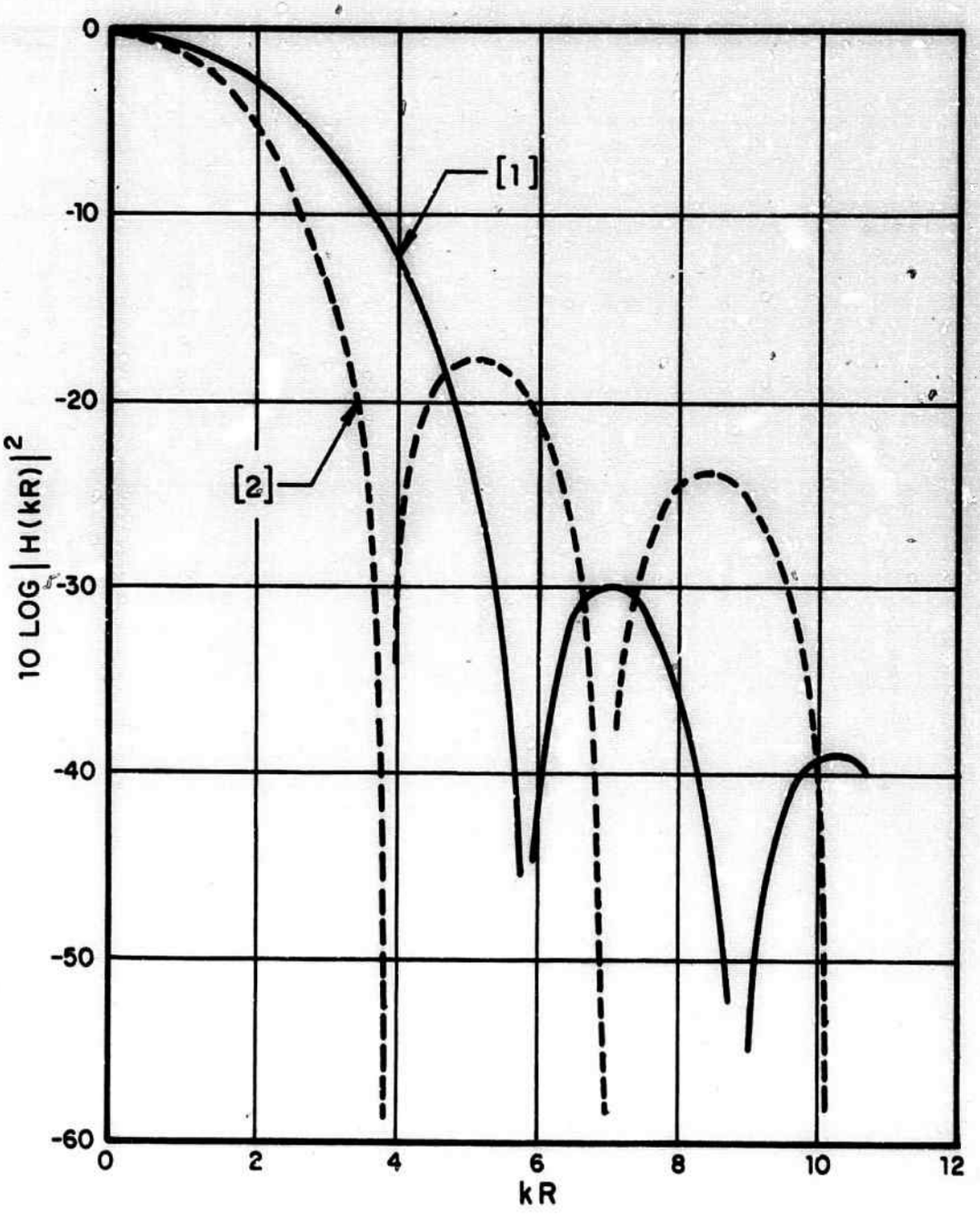

FIG.16

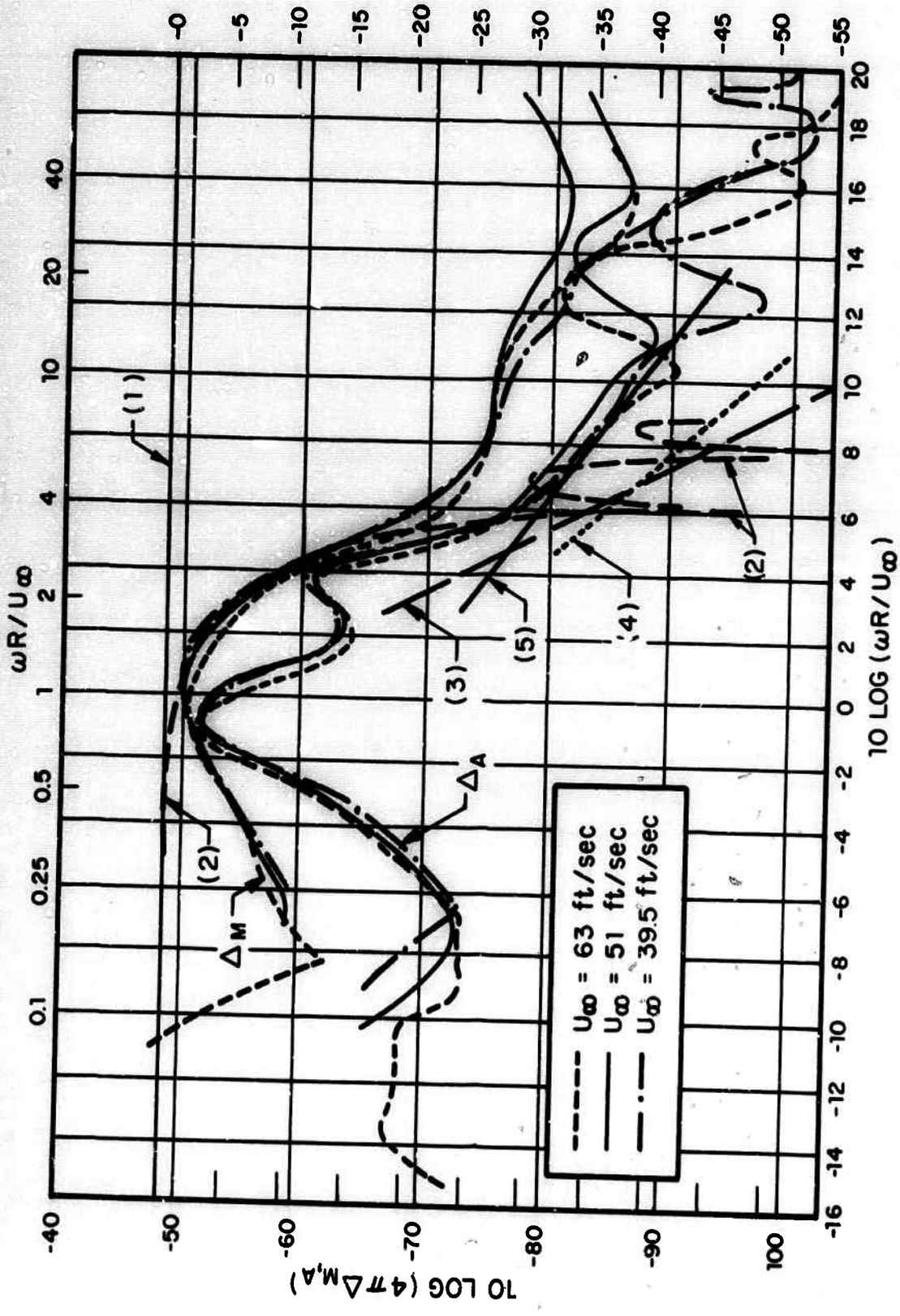
ωR/U∞
10 LOG (ωR/U∞)
10 LOG (4πΔM,A)
U∞ = 63 ft/sec
U∞ = 51 ft/sec
U∞ = 39.5 ft/sec
(1)
(2)
(3)
(4)
(5)
ΔM
ΔA

FIG. 17

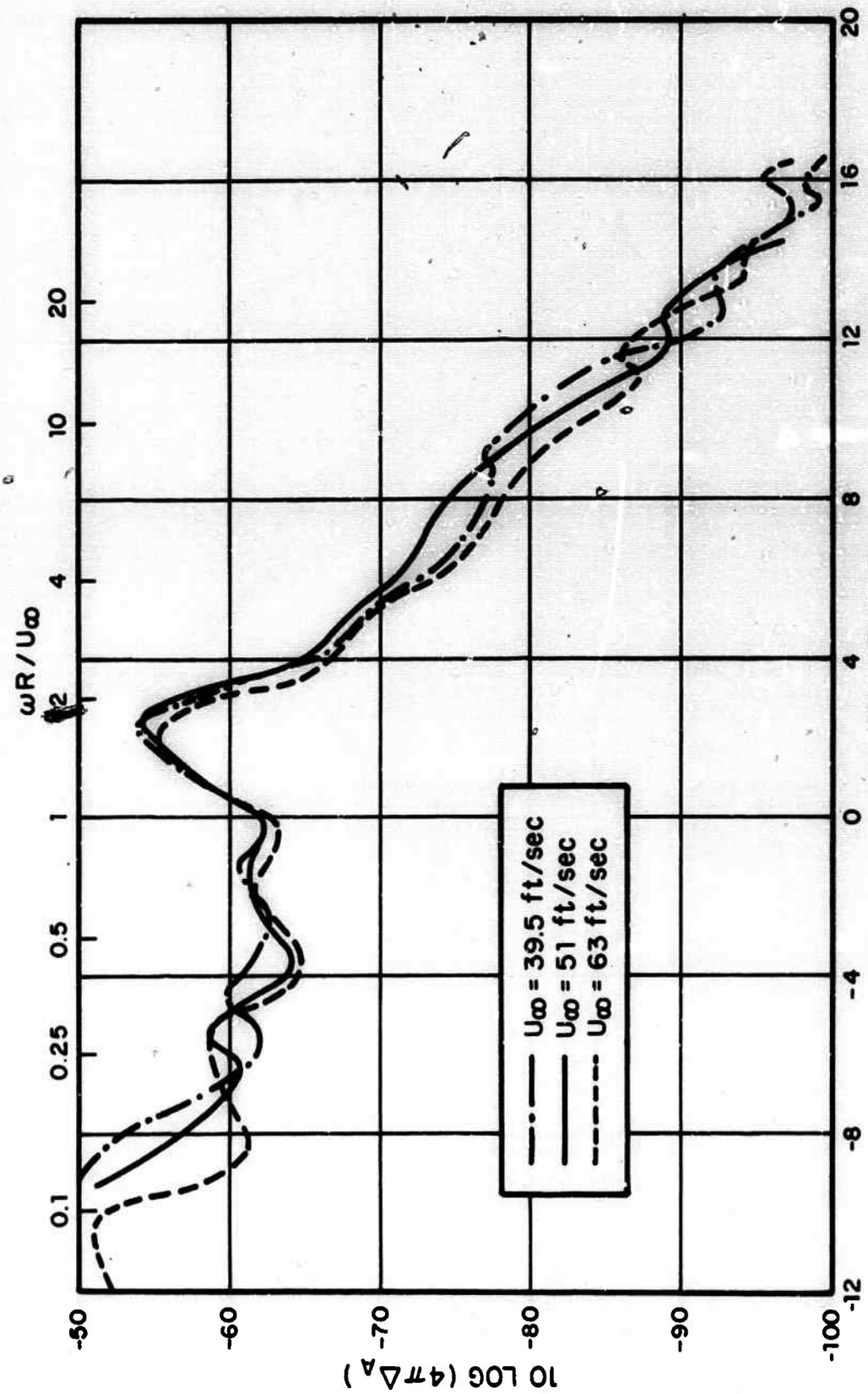
10 LOG (4πΔA)
-50
-60
-70
-80
-90
-100
ωR/U∞
0.1
0.25
0.5
1
2
4
10
20
10 LOG (ωR/U∞)
-12
-8
-4
0
4
8
12
16
20
U∞ = 39.5 ft/sec
U∞ = 51 ft/sec
U∞ = 63 ft/sec

FIG.18

BLANK PAGE

Unclassified
Security Classification

DOCUMENT CONTROL DATA - R & D

(Security classification of title, body of abstract and indexing annotation must be entered when the overall report is classified)

1. ORIGINATING ACTIVITY (Corporate author) Bolt Beranek and Newman Inc.	2a. REPORT SECURITY CLASSIFICATION Unclassified 2b. GROUP

3. REPORT TITLE
Wavenumber-Frequency Spectra of Turbulent-Boundary-Layer Pressure Measured by Microphone Arrays

4. DESCRIPTIVE NOTES (Type of report and inclusive dates)

5. AUTHOR(S) (First name, middle initial, last name)
William K. Blake and David M. Chase

6. REPORT DATE 25 April 1969	7a. TOTAL NO. OF PAGES 74	7b. NO. OF REFS 15
8a. CONTRACT OR GRANT NO. Nonr 3468(00) b. PROJECT NO. Task 2.3 c. d.	9a. ORIGINATOR'S REPORT NUMBER(S) 1769 9b. OTHER REPORT NO(S) (Any other numbers that may be assigned this report)	

10. DISTRIBUTION STATEMENT

11. SUPPLEMENTARY NOTES	12. SPONSORING MILITARY ACTIVITY Acoustics Branch, Code 468 Office of Naval Research

13. ABSTRACT Measurements of frequency spectra of pressure along a wind-tunnel wall have been made by single microphones and by a longitudinal array of four flush 0.8-inch circular microphones connected with alternating and with common phase. The alternating-phase array was designed to suppress by its wavenumber filtering the background acoustic duct noise at frequencies near 3 kHz. The measured levels set upper limits on low-wavenumber boundary-layer pressure. Analysis indicates that the high-wavenumber (convective) contribution in this frequency range was probably negligible, but it could not be definitely established whether background noise dominated the spectra or whether the upper bound set on low-wavenumber boundary-layer noise is a close one. On assumption of wavenumber independence in most of the pertinent low-wavenumber domain, an upper bound is given for the wavenumber spectral density of boundary-layer pressure, and its generalization by assumption of δ_*-independence is discussed. At lower frequencies, in identifiable domains where single-microphone and array spectra are dominated by the convective wavenumber component of boundary-layer pressure, satisfactory agreement is found with theoretical predictions based on current knowledge of the spectral density in the convective-wavenumber domain and on a measured facial sensitivity distribution for the microphone. In general, salient features of the array spectra correlate well with expectation, and the array technique is demonstrated to be a useful one for the subject purposes.

DD FORM 1 NOV 68 1473

Unclassified
Security Classification

14. KEY WORDS	LINK A		LINK B		LINK C	
	ROLE	WT	ROLE	WT	ROLE	WT
Turbulent boundary-layer pressure						
Wavenumber-frequency spectrum of pressure						
Arrays of microphones						
Wave-vector filter						